Supporting Information

for

Different Oxidative Addition Mechanisms for 12- and 14-Electron Palladium(0) Explain Ligand-Controlled Divergent Site Selectivity

*Jacob P. Norman,‡ Nathaniel G. Larson,‡ Sharon R. Neufeldt**

‡these authors contributed equally

Department of Chemistry and Biochemistry, Montana State University

Bozeman, MT 59717, USA

**Correspondence: sharon.neufeldt@montana.edu*

Table of Contents

I. Experimental Details

A. General Materials and Methods

NMR spectra were recorded at 298 K on a Bruker DRX 500 MHz (500.233 MHz for ^{1}H, 125.795 MHz for ^{13}C, 470.639 MHz for ^{19}F) or a Bruker Ascend 400 MHz (400.130 MHz for ^{1}H NMR, 100.613 for ^{13}C). ^{1}H and ^{13}C NMR chemical shifts are reported in parts per million (ppm) relative to TMS, with the residual solvent peak used as an internal reference [^{1}H NMR: $CHCl_3$ (7.26 ppm), C_6D_5H (7.16 ppm); ^{13}C NMR: $CDCl_3$ (77.16 ppm), ^{13}C NMR: C_6D_6 (128.06 ppm)]. Multiplicities are reported as follows: singlet (s), doublet (d), doublet of doublets (dd), and multiplet (m). GC data were collected using a Shimadzu GC-2010 Plus with a flame ionization detector equipped with a SH-Rxi-5ms capillary column (15 m x 0.25 mm ID x 0.25 μm df). GCMS data were collected with a Shimadzu GC-2030 paired with a Shimadzu GCMS-QP2020 NX and equipped with a SH-Rxi-5ms capillary column (30 m x 0.25 mm ID x 0.25 μm df). LC-MS analyses were performed on either an Agilent 6538 Q-TOF MS or a Bruker micro-TOF MS, both coupled to an Agilent 1290 Infinity UHPLC system. A 50 mm long Eclipse Plus C18 column (Agilent Technologies, Santa Barbara, CA; i.d. 2.1 mm, 1.8 μm particle size) was used for separation. A 6-minute gradient was used at a flow rate of 0.6 mL/min: 0-1 min 95% buffer A (100% H2O with 0.1% formic acid), followed by a gradient from 1-4 minutes of 5-95% buffer B (100% acetonitrile with 0.1% formic acid), 1 minute 95% buffer B, and returning to 95% buffer A for 1 minute. The mass spectrometers were operated in positive-ion mode with electrospray ionization.

Unless otherwise noted below, all commercially-obtained chemicals were used as received. (η^3-1-^{t}Bu-indenyl)Pd(IPr)(Cl) was obtained from Umicore. *N*-heterocyclic carbene ligands IMes, SIMes, IPr, or SIPr were each obtained from Strem Chemicals or Sigma Aldrich. Unless otherwise noted, dichloroheteroarenes and arylboronic acid starting materials were obtained from Oakwood Chemical. Arylated pyridines **2a**, **2b**, **S2c**, **S4b**, and **S5b** were prepared as previously reported.[1] 1,4-Dioxane, potassium *tert*-butoxide, and palladium (II) chloride were obtained from Acros Organics. Potassium carbonate, triphenylphosphine, and tri-*tert*-butylphosphine, were obtained from Alfa Aesar. THF, toluene, and methanol were obtained from Fisher Scientific. *tert*-butyl bromide, diphenylphosphinoferrocene, tri-*o*-tolylphosphine, and tricyclohexylphosphine were obtained from Oakwood chemical. Tri-*n*-butylphosphine was obtained from Sigma-Aldrich. Palladium (II) acetate, trimethyl phosphine, Q-Phos, CyJohnPhos, and CataCXium A were obtained from Strem Chemical. Benzene was obtained from Beantown Chemical. For the purpose of Suzuki-Miyaura cross-couplings, THF was used as received from Fisher Scientific. 1,4-Dioxane required for Pd/dppf-mediated Suzuki-Miyaura cross-couplings was used as received from Acros Organics but kept under N_2 prior to and during use.

Deuterated solvents ($CDCl_3$, C_6D_6) were obtained from Cambridge Isotopes and stored over molecular sieves. Manual flash column chromatography was performed on SiliCycle silica gel 60 (40-63 μm particle size) and thin layer chromatography was performed on SiliCycle TLC plates pre-coated with extra hard silica gel 60 F_{254}. Automated flash column chromatography was performed with a Biotage Selekt equipped with Biotage Sfär silica flash cartridges (20 μm particle size; 50 Å pore width) for normal phase separations, or Silica C18 cartridges (30 μm particle size; 100 Å pore width) for reversed phase separations.

B. General Procedure for Suzuki Cross-Couplings

GC-Scale Reactions. The specified solids required in the Suzuki-Miyaura reactions were added to a 1-dram reaction vial in order of increasing mass: palladium catalyst (palladium source and free ligand) or precatalyst, the specified dihalopyridine substrate if solid (0.08 mmol, 1 equiv), arylboronic acid (0.08 mmol, 1.0 equiv), potassium carbonate or cesium carbonate, and then a stir bar. Liquid reagents were pre-measured by syringe and added in quick succession: benzene, THF, or 1,4-dioxane (0.32 mL, 0.25 *M*) via 1-mL syringe, followed by N_2-sparged deionized water via 50-µL syringe. Note: dihalopyridine substrates were added last if liquid, via microliter syringe. A septum cap equipped with an N_2-ingas and outgassing needle was fastened to the 1-dram reaction vial and the headspace was sparged for 30-45 seconds. With continuous sparging, the vial was unscrewed from the septum cap and lowered while the cap was replaced with a PTFE-lined cap. The reaction was stirred vigorously at the specified temperature for the specified duration.

C. Ligand Screen with (cod)Pd(CH_2SiMe_3)$_2$ (Table 1), [(η^3-1-^{t}Bu-indenyl)Pd(Cl)]$_2$, and Pd(OAc)$_2$)

Overview and Discussion. The effect of phosphine sterics was evaluated in reactions in which free phosphine was combined with (cod)Pd(CH_2SiMe_3)$_2$ (as shown in the manuscript, Table 1), [(η^3-1-^{t}Bu-indenyl)Pd(Cl)]$_2$, or Pd(OAc)$_2$. In addition, NHC ligands were evaluated in combination with (cod)Pd(CH_2SiMe_3)$_2$ or Pd(OAc)$_2$, or as part of a pre-formed complex with structure (η^3-1-^{t}Bu-indenyl)Pd(NHC)(Cl).

Overall, the steric trends were comparable for all Pd sources. However, in the conditions with Pd(OAc)$_2$, a dependence of selectivity and yield on L:Pd ratio was seen for some ligands that was not seen when using (cod)Pd(CH_2SiMe_3)$_2$. This may reflect the ability of Pd(OAc)$_2$ to oxidize phosphines,[2] thereby leading to a much lower effective L:Pd ratio and a change in the nature of the active catalyst. Notably, when using PCy_3 in combination with both Pd(OAc)$_2$ and [(η^3-1-^{t}Bu-indenyl)Pd(Cl)]$_2$, selectivity switches for L:Pd = 1:1 compared to 2:1. This observation is consistent with prior evidence that PCy_3 can support both mono- and bisligated palladium[3] which are expected to give different selectivities. However, this effect is not seen when using (cod)Pd(CH_2SiMe_3)$_2$, and instead a slight preference for reaction at C4 is observed with both 5 and 10 mol % PCy_3. This observation seems to suggest a higher concentration of monoligated Pd(PCy_3) when using (cod)Pd(CH_2SiMe_3)$_2$ as the palladium source.

Table S1. Ligand Screen with (cod)Pd(CH_2SiMe_3)$_2$ (Table 1).[a]

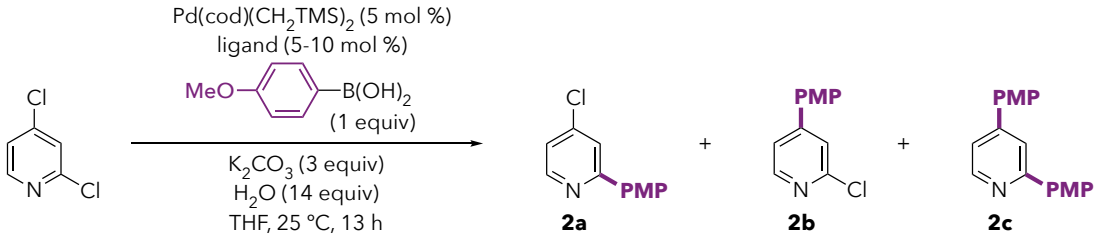

entry	trial	ligand (mol %)	%V_{bur} (min)[b]	**2a** (%)	**2b** (%)	**2c** (%)	**2a** : **2b**

1	1	PPh_3 (5)		83.9	0.5	0.1	>99 : 1
2	2	PPh_3 (5)		84.5	0.6	0.2	>99 : 1
3	Average	PPh_3 (5)	(28.2)	84.2	0.6	0.2	>99 : 1
4	1	PPh_3 (10)		82.8	0.3	0.1	>99 : 1
5	2	PPh_3 (10)		80.3	0.4	0.3	>99 : 1
6	Average	PPh_3 (10)	(28.2)	81.6	0.4	0.2	>99 : 1
7	1	P(*o*-tol)$_3$ (5)		39.1	22.0	4.2	1.8 : 1
8	2	P(*o*-tol)$_3$ (5)		44.8	20.9	3.4	2.1 : 1
9	Average	P(*o*-tol)$_3$ (5)	(34.4)	42.0	21.5	3.8	2.0 : 1
10	1	P(*o*-tol)$_3$ (10)		33.7	18.6	2.2	1.7 : 1
11	2	P(*o*-tol)$_3$ (10)		26.9	15.4	1.1	1.8 : 1
12	Average	P(*o*-tol)$_3$ (10)	(34.4)	30.3	17.0	1.7	1.8 : 1
13	1	PMe_3 (5)		18.8	2.2	0.4	8.5 : 1
14	2	PMe_3 (5)		18.3	2.2	0.4	8.3 : 1
15	Average	PMe_3 (5)	(22.1)	18.5	2.2	0.4	8.4 : 1
16	1	PMe_3 (10)		9.2	0.6	0.3	15.4 : 1
17	2	PMe_3 (10)		10.5	1.1	0.3	9.7 : 1
18	Average	PMe_3 (10)	(22.1)	9.9	0.9	0.3	11.0 : 1
19	1	P(*n*-Bu)$_3$ (5)		21.6	7.4	0.7	2.9 : 1
20	2	P(*n*-Bu)$_3$ (5)		18.4	7.8	0.7	2.4 : 1
21	Average	P(*n*-Bu)$_3$ (5)	(24.2)	20.0	7.6	0.7	2.6 : 1
22	1	P(*n*-Bu)$_3$ (10)		0.8	0.3	0.3	3.2 : 1
23	2	P(*n*-Bu)$_3$ (10)		0.7	0.2	0.3	3.2 : 1
24	Average	P(*n*-Bu)$_3$ (10)	(24.2)	0.8	0.3	0.3	3.2 : 1
25	1	PCy_3 (5)		26.3	42.0	4.7	1 : 1.6
26	2	PCy_3 (5)		29.4	47.7	5.9	1 : 1.6
27	Average	PCy_3 (5)	(30.2)	27.9	44.9	5.3	1 : 1.6
28	1	PCy_3 (10)		27.2	39.0	2.6	1 : 1.4
29	2	PCy_3 (10)		27.2	40.7	3.6	1 : 1.5
30	Average	PCy_3 (10)	(30.2)	27.2	39.9	3.1	1 : 1.5
31	1	PAd_2(*n*-Bu) (5)		24.4	53.0	6.5	1 : 2.2
32	2	PAd_2(*n*-Bu) (5)		23.7	50.7	10.0	1 : 2.1
33	Average	PAd_2(*n*-Bu) (5)	(32.8)	24.1	51.8	8.2	1 : 2.2
34	1	PAd_2(*n*-Bu) (10)		26.4	48.6	10.2	1 : 1.8
35	1	P^tBu_3 (5)		26.8	46.7	9.6	1 : 1.7
36	2	P^tBu_3 (5)		27.1	47.8	11.9	1 : 1.8
37	Average	P^tBu_3 (5)	(36.3)	27.0	47.3	10.8	1 : 1.8
38	1	P^tBu_3 (10)		27.1	47.5	8.9	1 : 1.7
39	1	QPhos (5)		23.4	48.2	5.4	1 : 2.1
40	2	QPhos (5)		24.7	52.0	6.9	1 : 2.1
41	Average	QPhos (5)	(47.6)	24.1	50.1	6.2	1 : 2.1
42	1	IMes (5)		33.9	50.8	4.9	1 : 1.5
43	2	IMes (5)		31.0	53.3	8.1	1 : 1.7
44	Average	IMes (5)	36.5	32.5	52.0	6.5	1 : 1.6
45	1	SIMes (5)		27.2	21.3	0.7	1.3 : 1
46	2	SIMes (5)		28.5	22.6	0.8	1.3 : 1
47	Average	SIMes (5)	36.9	27.9	22.0	0.8	1.3 : 1
48	1	IPr (5)		8.8	65.7	13.8	1 : 7.4
49	2	IPr (5)		10.1	67.9	6.7	1 : 6.7
50	Average	IPr (5)	44.5	9.5	66.8	10.3	1 : 7.0
51	1	SIPr (5)		9.3	35.5	3.5	3.8 : 1
52	2	SIPr (5)		9.6	37.3	3.4	3.9 : 1
53	Average	SIPr (5)	47.0	9.5	36.4	3.5	3.8 : 1

[a] Reactions were conducted according to the General Procedure for GC-scale reactions. GC yields calibrated against undecane as an internal standard. [b]Values in parentheses are minimum percent buried volumes obtained from the Kraken database.[4] Percent buried volumes of NHCs reported for LAuCl complexes at a L–Au distance of 2.00 Å from reference 5.

Table S2. Ligand Screen with [(η³-1-ᵗBu-indenyl)Pd(Cl)]₂ (**I**) and (η³-1-ᵗBu-indenyl)Pd(NHC)(Cl) (**II**).[a]

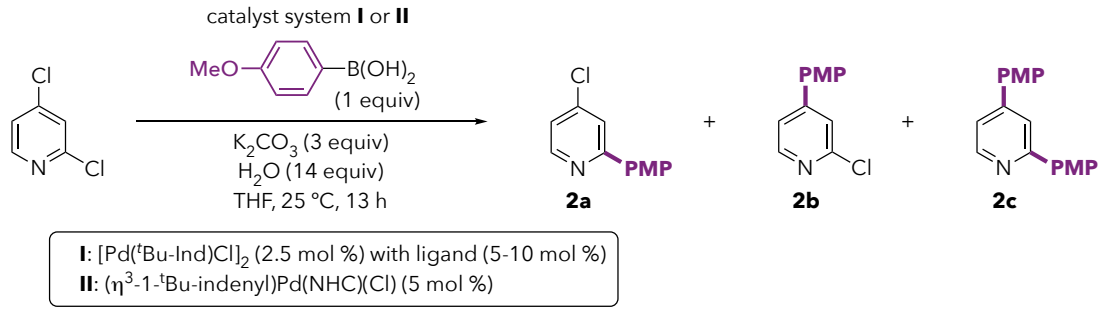

entry	trial	Pd source	ligand (mol %)	%V_{bur} (min)[b]	**2a** (%)	**2b** (%)	**2c** (%)	**2a** : **2b**
1	1	**I**	PPh_3 (5)		77.4	0.3	0.1	>99 : 1
2	2	**I**	PPh_3 (5)		74.1	0.4	n.d.	>99 : 1
3	Average	**I**	PPh_3 (5)	(28.2)	75.7	0.4	0.1	>99 : 1
4	1	**I**	PPh_3 (10)		77.7	0.3	0.1	>99 : 1
5	2	**I**	PPh_3 (10)		64.6	0.4	n.d.	>99 : 1
6	Average	**I**	PPh_3 (10)	(28.2)	71.2	0.4	0.1	>99 : 1
7	1	**I**	P(*o*-tol)$_3$ (5)		24.4	13.7	0.9	1.8 : 1
8	2	**I**	P(*o*-tol)$_3$ (5)		28.2	17.1	1.3	1.6 : 1
9	Average	**I**	P(*o*-tol)$_3$ (5)	(34.4)	26.3	15.4	1.1	1.7: 1
10	1	**I**	P(*o*-tol)$_3$ (10)		9.3	6.4	0.1	1.5 : 1
11	2	**I**	P(*o*-tol)$_3$ (10)		17.4	11.9	0.4	1.5 : 1
12	Average	**I**	P(*o*-tol)$_3$ (10)	(34.4)	13.4	9.1	0.3	1.5 : 1
13	1	**I**	PMe_3 (5)		4.7	0.5	n.d.	8.7 : 1
14	2	**I**	PMe_3 (5)		4.4	0.5	n.d.	9.2 : 1
15	Average	**I**	PMe_3 (5)	(22.1)	4.6	0.5	n.d.	9.0 : 1
16	1	**I**	PMe_3 (10)		6.1	0.4	n.d.	16.5 : 1
17	2	**I**	PMe_3 (10)		7.6	0.4	n.d.	21.4: 1
18	Average	**I**	PMe_3 (10)	(22.1)	6.8	0.4	n.d.	18.9 : 1
19	1	**I**	P(*n*-Bu)$_3$ (5)		3.1	0.6	n.d.	5.2 : 1
20	2	**I**	P(*n*-Bu)$_3$ (5)		2.1	0.4	n.d.	5.3: 1
21	Average	**I**	P(*n*-Bu)$_3$ (5)	(24.2)	2.6	0.5	n.d.	5.3 : 1
22	1	**I**	P(*n*-Bu)$_3$ (10)		2.3	0.4	n.d.	5.8 : 1
23	2	**I**	P(*n*-Bu)$_3$ (10)		1.6	0.2	n.d.	6.8 : 1
24	Average	**I**	P(*n*-Bu)$_3$ (10)	(24.2)	2.0	0.3	n.d.	6.7 : 1
25	1	**I**	PCy_3 (5)		13.1	21.8	0.8	1 : 1.7
26	2	**I**	PCy_3 (5)		23.4	37.9	3.5	1 : 1.6
27	Average	**I**	PCy_3 (5)	(30.2)	18.3	29.9	2.2	1 : 1.7
28	1	**I**	PCy_3 (10)		0.4	0.1	n.d.	4.0 : 1
29	2	**I**	PCy_3 (10)		0.4	0.1	n.d.	4.0 : 1
30	Average	**I**	PCy_3 (10)	(30.2)	0.4	0.1	n.d.	4.0 : 1
31	1	**I**	PAd_2(*n*-Bu) (5)		21.4	43.8	4.9	1 : 2.0
32	2	**I**	PAd_2(*n*-Bu) (5)		21.4	46.3	6.0	1 : 2.2
33	Average	**I**	PAd_2(*n*-Bu) (5)	(32.8)	21.4	45.1	5.5	1 : 2.1
34	1	**I**	PAd_2(*n*-Bu) (10)	(32.8)	1.7	2.6	1.4	1 : 1.5
35	1	**I**	P^{t}Bu$_3$ (5)		24.6	43.1	6.2	1 : 1.7
36	2	**I**	P^{t}Bu$_3$ (5)		26.9	46.6	8.0	1 : 1.7
37	Average	**I**	P^{t}Bu$_3$ (5)	(36.3)	25.8	44.9	7.1	1 : 1.7
38	1	**I**	P^{t}Bu$_3$ (10)	(36.3)	18.6	31.4	3.5	1 : 1.7
39	1	**I**	Q-Phos (5)		23.0	47.2	5.7	1 : 2.1
40	2	**I**	Q-Phos (5)		23.2	49.4	6.9	1 : 2.1
41	Average	**I**	Q-Phos (5)	(47.6)	23.1	48.3	6.3	1 : 2.1
42	1	**II**	IMes		31.6	39.7	1.7	1 : 1.3

43	2	**II**	IMes		29.7	37.0	1.3	1 : 1.2
44	Average	**II**	IMes	36.5	30.7	38.4	1.5	1 : 1.3
48	1	**II**	SIMes		37.6	36.9	1.4	1.1 : 1
49	2	**II**	SIMes		38.6	38.8	1.3	1 : 1.0
50	Average	**II**	SIMes	36.9	38.1	37.9	1.4	1 : 1.0
51	1	**II**	IPr		6.6	68.8	4.0	1 : 10.4
52	2	**II**	IPr		6.5	70.1	4.3	1 : 10.8
53	Average	**II**	IPr	44.5	6.6	69.5	4.2	1 : 10.6
54	1	**II**	SIPr		7.2	70.9	7.7	1 : 9.8
55	2	**II**	SIPr		6.6	67.7	7.1	1 : 10.2
56	Average	**II**	SIPr	47.0	6.9	69.3	7.4	1 : 10.0

[a] Reactions were conducted according to the General Procedure for GC-scale reactions. GC yields calibrated against undecane as an internal standard. [b]Values in parentheses are minimum percent buried volumes obtained from the Kraken database.[4] Percent buried volumes of NHCs reported for LAuCl complexes at a L–Au distance of 2.00 Å from reference 5.

Table S3. Ligand Screen with $Pd(OAc)_2$[a]

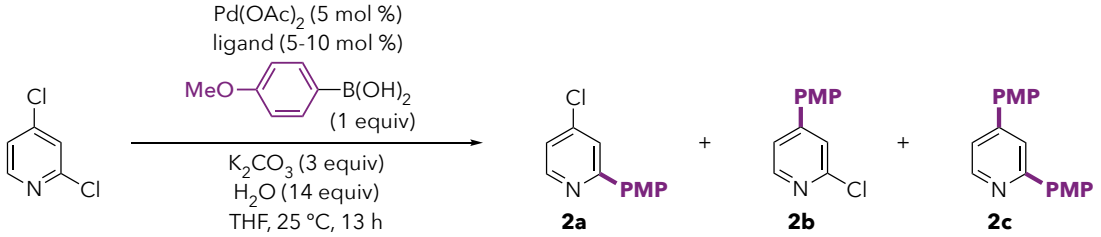

entry	trial	ligand (mol %)	%V_{bur} (min)[b]	**2a** (%)	**2b** (%)	**2c** (%)	**2a** : **2b**
1	1	PPh_3 (5)		5.5	0.9	1.5	6.1 : 1
2	2	PPh_3 (5)		6.4	0.6	1.6	10.7 : 1
3	Average	PPh_3 (5)	(28.2)	6.0	0.7	1.6	8.6 : 1
4	1	PPh_3 (10)		64.6	0.4	n.d.	>99 : 1
5	2	PPh_3 (10)		64.6	0.4	n.d.	>99 : 1
6	Average	PPh_3 (10)	(28.2)	63.3	0.4	n.d.	>99 : 1
7	1	P(*o*-tol)$_3$ (5)		20.8	10.4	1.8	2.0 : 1
8	2	P(*o*-tol)$_3$ (5)		20.5	10.7	1.7	1.9 : 1
9	Average	P(*o*-tol)$_3$ (5)	(34.4)	20.7	10.6	1.8	2.0 : 1
10	1	P(*o*-tol)$_3$ (10)		7.2	4.1	1.0	1.8 : 1
11	2	P(*o*-tol)$_3$ (10)		10.2	5.9	1.7	1.7 : 1
12	Average	P(*o*-tol)$_3$ (10)	(34.4)	8.7	5.0	1.4	1.7 : 1
13	1	PMe_3 (5)		2.8	0.2	n.d.	14.0 : 1
14	2	PMe_3 (5)		6.9	0.8	n.d.	8.6 : 1
15	Average	PMe_3 (5)	(22.1)	4.9	0.5	n.d.	9.8 : 1
16	1	PMe_3 (10)		8.3	0.9	n.d.	9.2 : 1
17	2	PMe_3 (10)		6.9	0.6	n.d.	11.5 : 1
18	Average	PMe_3 (10)	(22.1)	7.6	0.8	n.d.	9.5 : 1
19	1	P(*n*-Bu)$_3$ (5)		6.3	1.0	n.d.	6.3 : 1
20	2	P(*n*-Bu)$_3$ (5)		9.0	2.2	n.d.	4.1 : 1
21	Average	P(*n*-Bu)$_3$ (5)	(24.2)	7.7	1.6	n.d.	4.8 : 1
22	1	P(*n*-Bu)$_3$ (10)		5.1	0.7	n.d.	7.3 : 1
23	2	P(*n*-Bu)$_3$ (10)		6.3	1.0	n.d.	6.3 : 1
24	Average	P(*n*-Bu)$_3$ (10)	(24.2)	5.7	0.9	n.d.	6.3 : 1
25	1	PCy_3 (5)		11.5	16.0	2.0	1 : 1.4
26	2	PCy_3 (5)		9.6	15.7	1.6	1 : 1.6
27	Average	PCy_3 (5)	(30.2)	10.6	15.9	1.8	1 : 1.5
28	1	PCy_3 (10)		2.6	1.2	2.3	2.2 : 1

29	2	PCy_3 (10)		2.9	0.8	1.2	3.6 : 1
30	Average	PCy_3 (10)	(30.2)	2.7	1.0	1.8	2.7 : 1
31	1	CyJohnPhos (5)		28.9	15.9	3.7	1.8 : 1
32	2	CyJohnPhos (5)		26.5	14.0	3.0	1.9 : 1
33	Average	CyJohnPhos (5)	(31.8)	27.7	14.9	3.3	1.9 : 1
34	1	PAd_2(*n*-Bu) (5)		17.6	33.0	3.0	1 : 1.9
35	2	PAd_2(*n*-Bu) (5)		21.8	43.5	3.9	1 : 2.0
36	Average	PAd_2(*n*-Bu) (5)	(32.8)	19.7	38.3	3.4	1 : 1.9
37	1	PAd_2(*n*-Bu) (10)	(32.8)	21.6	45.6	7.1	1 : 2.1
38	1	P^tBu_3 (5)		26.9	44.3	8.7	1 : 1.7
39	2	P^tBu_3 (5)		22.1	33.7	4.3	1 : 1.5
40	Average	P^tBu_3 (5)	(36.3)	24.5	39.0	6.5	1 : 1.6
41	1	P^tBu_3 (10)	(36.3)	27.7	39.7	7.7	1 : 1.4
42	1	Q-Phos (5)		22.8	40.5	4.2	1 : 1.8
43	2	Q-Phos (5)		22.9	41.1	4.7	1 : 1.8
44	Average	Q-Phos (5)	(47.6)	22.9	40.8	4.4	1 : 1.8
45	1	Q-Phos (10)	(47.6)	24.2	45.8	6.7	1 : 1.9
46	1	IMes (5)		26.6	27.1	2.5	1 : 1
47	2	IMes (5)		25.9	26.3	2.5	1 : 1
48	Average	IMes (5)	36.5	26.2	26.7	2.5	1 : 1
49	1	SIMes (5)		8.5	7.3	1.5	1.2 : 1
50	2	SIMes (5)		13.2	10.6	2.0	1.2 : 1
51	Average	SIMes (5)	36.9	10.8	8.9	1.8	1.2 : 1
52	1	IPr (5)		4.3	22.8	3.4	1 : 5.3
53	2	IPr (5)		5.2	37.2	5.2	1 : 7.2
54	Average	IPr (5)	44.5	4.8	30.0	4.3	1 : 6.3
55	1	SIPr (5)		2.9	4.9	1.5	1 : 1.7
56	2	SIPr (5)		4.9	7.7	2.1	1 : 1.6
57	Average	SIPr (5)	47.0	3.9	6.3	1.8	1 : 1.6

[a] Reactions were conducted according to the General Procedure for GC-scale reactions. GC yields calibrated against undecane as an internal standard. [b]Values in parentheses are minimum percent buried volumes obtained from the Kraken database.[4] Percent buried volumes of NHCs reported for LAuCl complexes at a L–Au distance of 2.00 Å from reference 5.

D. Influence of 6-Substituent on Selectivity with IMes (Scheme 2A) and IPr

Table S4. Effect of 6-Substituent on Selectivity in Benzene (Scheme 2A)[a]

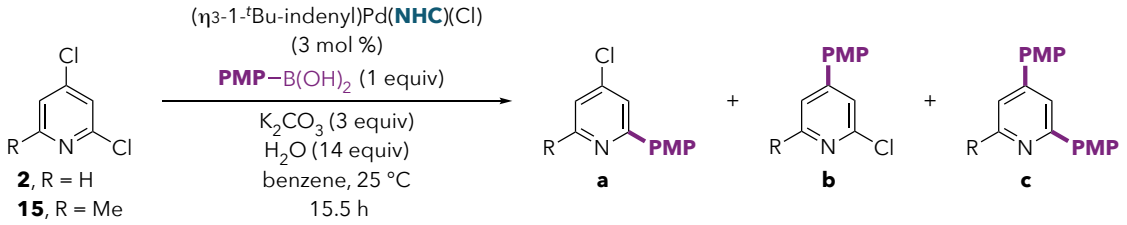

entry	trial	NHC	-R	**a** (%)	**b** (%)	**c** (%)	**a** : **b**
1	1	IMes	H	21	35	3	1 : 1.7
2	2	IMes	H	25	44	3	1 : 1.8
3	Average	IMes	H	23	40	3	1 : 1.7
4	1	IMes	Me	15	55	4	1: 3.7
5	2	IMes	Me	15	57	6	1 : 3.8
6	Average	IMes	Me	15	56	5	1 : 3.7
7	1	IPr	H	8	69	6	1 : 8.6

8	2	IPr	H	8	72	5	1 : 9.0
9	Average	IPr	H	8	71	6	1 : 8.8
10[b]	1	IPr	Me	3	45	21	1 : 15

[a]Reactions were conducted according to the General Procedure for GC-scale reactions. GC yields calibrated against undecane as an internal standard. [b]Reaction run for 13 h.

Table S5. Effect of 6-Substituent on Selectivity in THF[a]

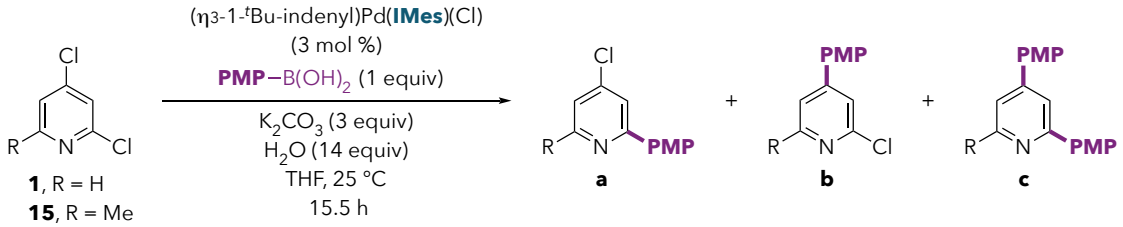

entry	trial	-R	**a** (%)	**b** (%)	**c** (%)	**a** : **b**
1	1	H	36	47	4	1 : 1.3
2	2	H	49	38	5	1.3 : 1
3	Average	H	43	43	4	1 : 1
4[b]	1	CF_3	34	56	11	1 : 1.5
5[b]	2	CF_3	34	60	14	1 : 1.8
6[b]	Average	CF_3	34	58	12	1: 1.7
7	1	Me	23	56	11	1 : 2.4
8	2	Me	21	55	11	1 : 2.6
9	Average	Me	22	56	11	1 : 2.5

[a]Reactions were conducted according to the General Procedure for GC-scale reactions. Unless otherwise noted, yields are GC yields calibrated against undecane as an internal standard. [b]Uncalibrated GC yields.

E. Influence of [2] on Selectivity with IMes (Scheme 2B), IPr, and P^{t}Bu$_3$

Overview and Discussion. The selectivity of (η^3-1-^{t}Bu-indenyl)Pd(IMes)(Cl) is sensitive to the concentration of substrate **2** (Table S6). At higher [**2**], more reaction at C2 is seen, consistent with greater availability of **2** that can coordinate to Pd(IMes) leading to preferential reaction at C2 through a bisligated transition state **TS13a-IMes**.

For comparison, no change or only a slight change in selectivity is seen in analogous experiments using (η^3-1-^{t}Bu-indenyl)Pd(**IPr**)(Cl) (Table S7) and (cod)Pd(CH_2SiMe_3)$_2$/**P^{t}Bu$_3$** (Table S8). With both catalytic systems, DFT calculations predict that reaction at C4 is favored through monoligated PdL, but that *if* bisligated PdL(**2**) could react, it would prefer C2. For the former catalytic system, reaction of C2—Cl at Pd(IPr)(**2**) (**TS13a-IPr**) is calculated to be disfavored over the monoligated TS for reaction at C4 (**TS10b-IPr**) by 4.0 kcal/mol. In the latter system, reaction at C2 at Pd(P^{t}Bu$_3$)(**2**) is disfavored by 10.1 kcal/mol (see Figure 1 in the manuscript, compare **TS13a-PtBu3** to **TS10b-PtBu3**). These trends are consistent with the very slight sensitivity of the Pd/IPr system to [**2**], and the nonexistent sensitivity of the Pd/P^{t}Bu$_3$ system to [**2**].

Table S6. Influence of [**2**] on Selectivity with IMes (Scheme 2B)[a]

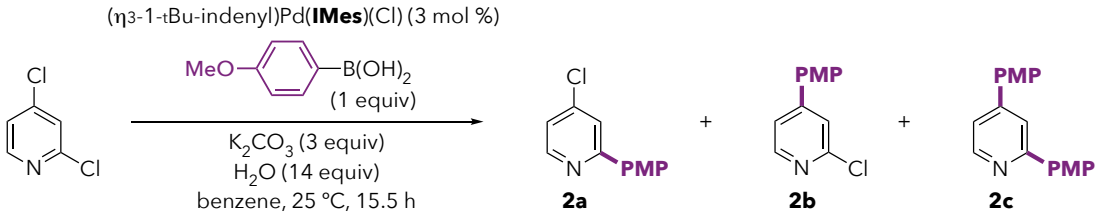

entry	Trial	**2** (equiv)	**2a** (%)	**2b** (%)	**2c** (%)	2a : 2b	$\Delta\Delta G^{\ddagger}_{(C4\text{-}C2)}$ (kcal/mol)[b]
1	1	1	21.1	35.3	2.7	1 : 1.7	-0.3
2	2	1	24.3	44.0	3.0	1 : 1.8	-0.3
3	Average	1	22.7	39.7	2.9	1 : 1.7	-0.3
4	1	2	28.6	27.5	0.8	1 : 1.0	0.0
5	2	2	33.2	31.1	1.0	1.1 : 1	0.0
6	Average	2	30.9	29.3	0.9	1.1 : 1	0.0
7	1	5	32.3	10.4	0.7	3.1 : 1	+0.7
8	2	5	43.8	17.9	0.6	2.4 : 1	+0.5
9	Average	5	38.1	14.2	0.7	2.7 : 1	+0.6
10	1	10	42.0	8.8	0.9	4.8 : 1	+0.9
11	2	10	43.8	9.6	0.4	4.6 : 1	+0.9
12	Average	10	42.9	9.2	0.7	4.7 : 1	+0.9

[a]Reactions were conducted according to the General Procedure for GC-scale reactions. GC yields calibrated against undecane as an internal standard. [b]Difference in free energies of activation for reaction at C4 versus C2 calculated from the experimental product ratios using the Eyring equation at 298.15 K.

Table S7. Influence of [**2**] on Selectivity with IPr[a]

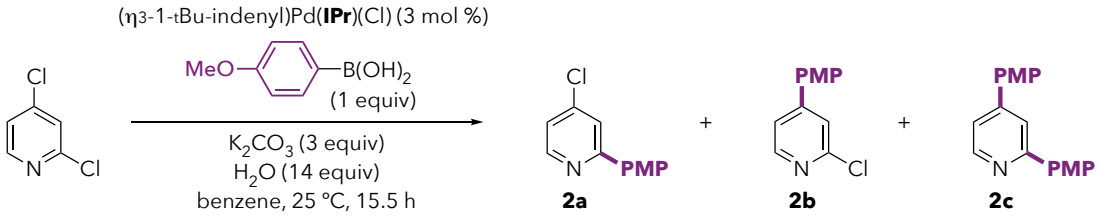

entry	Trial	**2** (equiv)	**2a** (%)	**2b** (%)	**2c** (%)	2a : 2b	$\Delta\Delta G^{\ddagger}_{(C4\text{-}C2)}$ (kcal/mol)[b]
1	1	1	8.1	69.0	6.0	1 : 8.5	-1.3
2	2	1	8.6	70.5	6.4	1 : 8.2	-1.3
3	Average	1	8.3	69.7	6.2	1 : 8.4	-1.3
4	1	2	10.0	75.2	1.9	1 : 7.5	-1.2
5	2	2	9.1	70.1	1.7	1 : 7.7	-1.2
6	Average	2	9.6	72.6	1.8	1 : 7.6	-1.2
7	1	5	9.9	68.9	0.8	1 : 7.0	-1.2
8	2	5	9.8	70.9	0.8	1 : 7.2	-1.2
9	Average	5	9.9	69.9	0.8	1 : 7.1	-1.2
10	1	10	12.2	74.8	0.6	1 : 6.1	-1.1
11	2	10	10.2	65.7	0.6	1 : 6.4	-1.1
12	Average	10	11.2	70.3	0.6	1 : 6.3	-1.1

[a]Reactions were conducted according to the General Procedure for GC-scale reactions. GC yields calibrated against undecane as an internal standard. [b]Difference in free energies of activation for reaction at C4 versus C2 calculated from the experimental product ratios using the Eyring equation at 298.15 K.

Table S8. Influence of [**2**] on Selectivity with P^tBu_3[a]

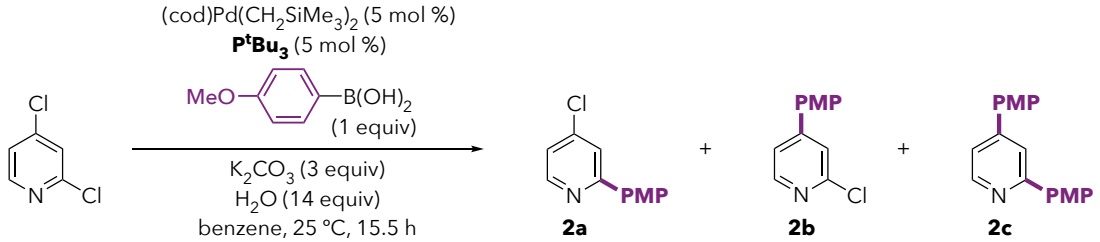

entry	Trial	**2** (equiv)	**2a** (%)	**2b** (%)	**2c** (%)	2a : 2b	$\Delta\Delta G^{\ddagger}_{(C4\text{-}C2)}$ (kcal/mol)[b]
1	1	1	29.3	49.0	14.4	1 : 1.7	-0.3
2	2	1	29.3	46.6	12.7	1 : 1.6	-0.3
3	Average	1	29.3	47.8	13.6	1 : 1.7	-0.3
4	1	2	31.9	50.8	4.8	1 : 1.6	-0.3
5	2	2	38.1	60.5	5.3	1 : 1.6	-0.3
6	Average	2	35.0	55.7	5.1	1 : 1.6	-0.3
7	1	5	39.1	62.0	1.9	1 : 1.6	-0.3
8	2	5	37.0	61.5	1.4	1 : 1.7	-0.3
9	Average	5	38.1	61.8	1.7	1 : 1.7	-0.3
10	1	10	37.1	63.4	1.0	1 : 1.7	-0.3
11	2	10	36.8	58.9	1.1	1 : 1.6	-0.3
12	Average	10	37.0	61.2	1.1	1 : 1.7	-0.3

[a]Reactions were conducted according to the General Procedure for GC-scale reactions. GC yields calibrated against undecane as an internal standard. [b]Difference in free energies of activation for reaction at C4 versus C2 calculated from the experimental product ratios using the Eyring equation at 298.15 K.

F. Selectivity Analysis of Substrates in Scheme 2C

Cross-coupling reactions of the substrates in Scheme 2C were set up according to the General Procedure for GC-scale reactions using (η^3-1-^{t}Bu-indenyl)Pd(IPr)(Cl) (3 mol%), K_2CO_3 (3 equiv), and deionized H_2O (14 equiv) at 60 °C in THF with stirring for 12 h. Reaction outcomes were analyzed by GC and GCMS using *n*-undecane as an internal standard. Solvent was removed from the reaction vials under vacuum, then the crude solids were redissolved in $CDCl_3$ or C_6D_6, filtered through celite, and analyzed by ^{1}H NMR. The unconventional monoarylated products of each reaction in Scheme 2C were isolated and fully characterized as described below in Section G, or they were isolated and characterized previously.[1] GC and ^{1}H NMR signals present in the crude reaction mixtures were identified based on comparison to those of the isolated products. The GC retention times of the diarylated products were assigned based on their mass values obtained by GCMS analysis. Where relevant, NMR yields of minor products were calculated from NMR signal ratios relative to the major product, whose yield was determined by calibrated GC analysis.

The Pd/IPr-catalyzed Suzuki cross-coupling of 3,5-dichloropyridazine (**5**) favors reaction at C5 according to crude GC, GCMS, and ^{1}H NMR analyses (ratio of **S5a** and **S5b** = 1 : 13.1 based on the ratio of signal integrations by ^{1}H NMR (C_6D_6, 500 MHz, Scheme S1B). As discussed in the manuscript, the difference in LUMO coefficient between C3 and C5 is substantial, consistent with high selectivity for the C5-site.

Scheme S1. Suzuki reaction of 5 using a Pd/IPr catalyst. (A) GC chromatogram of the crude reaction mixture. (B) Relevant region of the ^{1}H NMR spectrum of the crude reaction mixture.

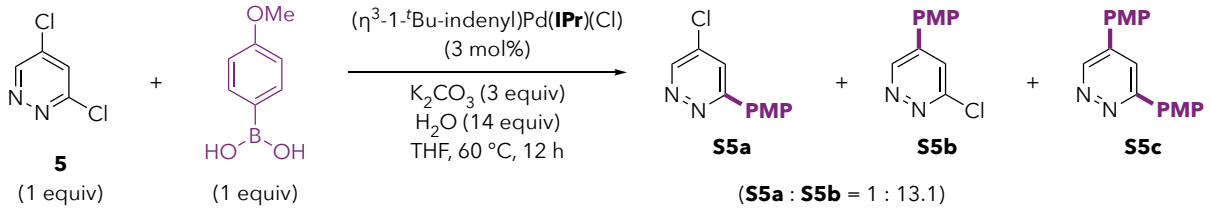

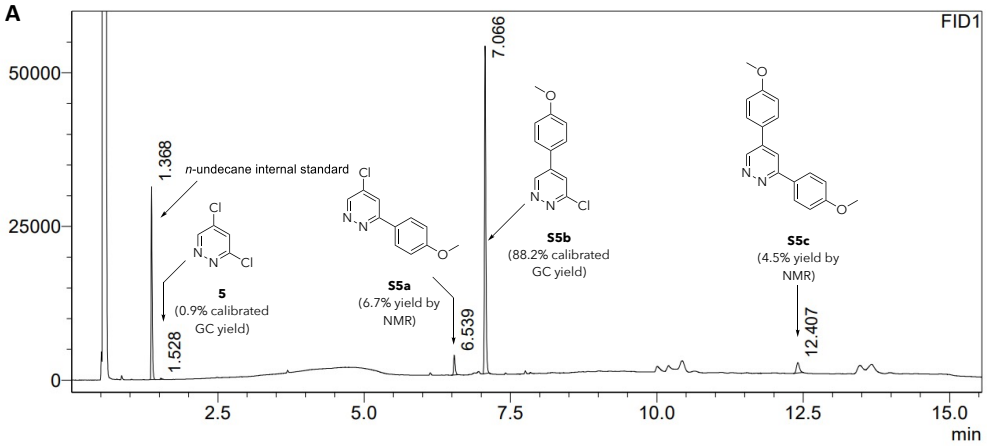

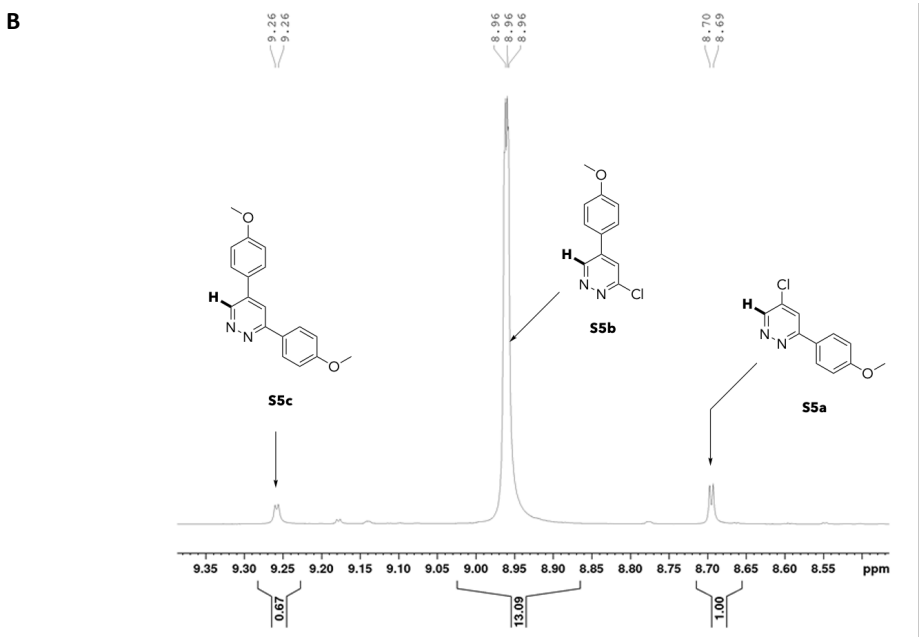

The Pd/IPr-catalyzed Suzuki cross-coupling of 2,4-dichloropyridine (**2**) favors reaction at C4 according to crude GC, GCMS, and ^{1}H-NMR analyses (ratio of **2a** and **2b** = 1 : 11.78 based on the ratio of signal integrations by ^{1}H-NMR ($CDCl_3$, 400 MHz, Scheme S2B), and 1 : 11.82 based on the ratio of calibrated signal integrations by GC, Scheme S2A). As discussed in the manuscript, the difference in LUMO coefficient between C2 and C4 is substantial, consistent with high selectivity for the C4-site.

Scheme S2. Suzuki reaction of **2** using a Pd(IPr) catalyst.

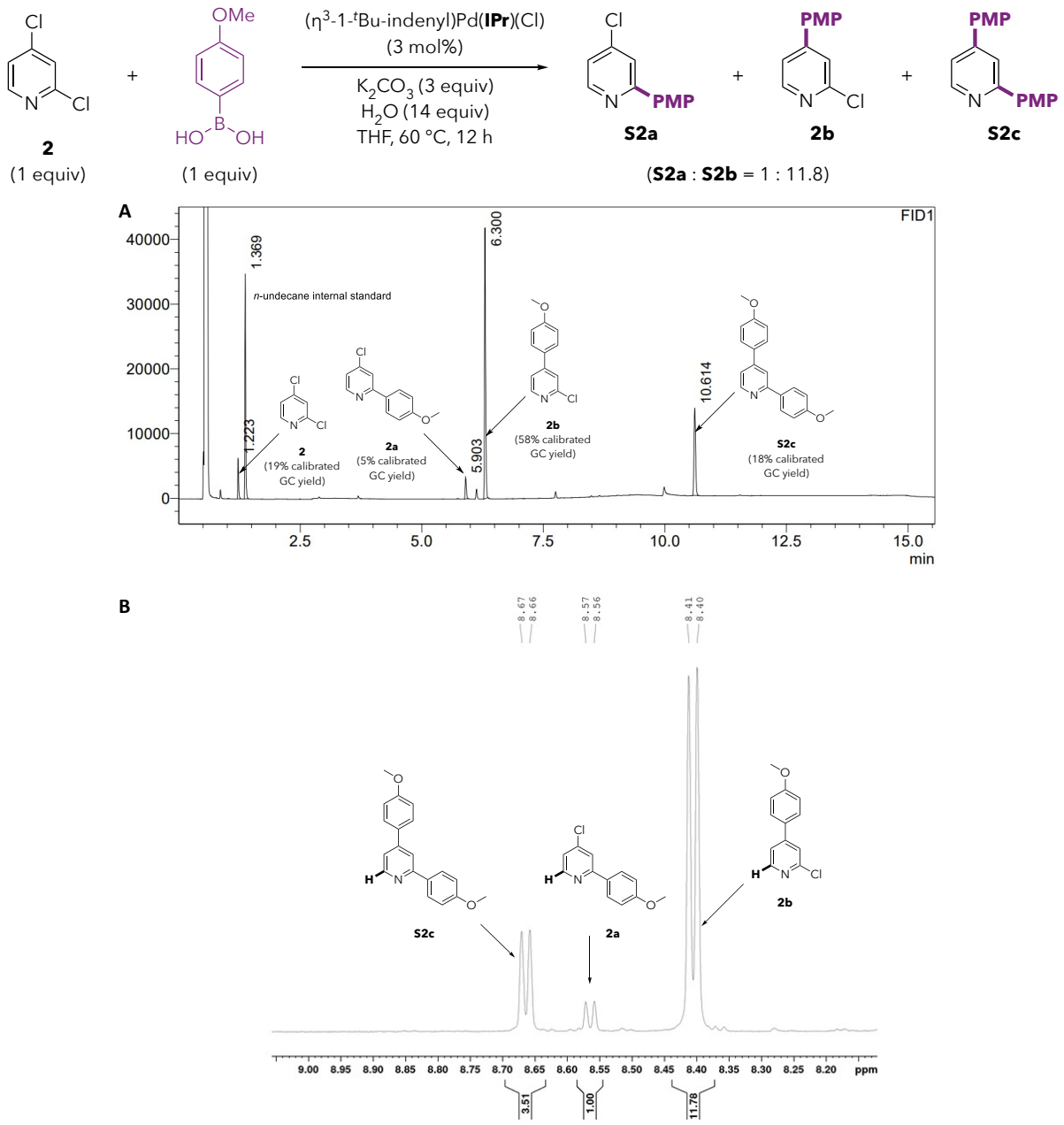

The Pd/IPr-catalyzed Suzuki cross-coupling of 2,3-dichloropyridine (**1**) favors reaction at the unconventional site C3 under the optimized system according to crude GC and GCMS analysis (ratio of **S1a** and **S1b** = 1 : 1.9 based on the ratio of signal integrations by ^{1}H-NMR ($CDCl_3$, 400 MHz, Scheme S3B). As such, the use of (η^3-1-^{t}Bu-indenyl)Pd(IPr)(Cl) promotes reaction at the site distal to nitrogen, albeit in low selectivity. As discussed in the manuscript, the difference in LUMO coefficient between C2 and C3 is modest, thus the reaction is not as selective as the reactions of 2,4-dichloropyridine or 3,5-dichloropyridazine.

Scheme S3. Suzuki reaction of **1** using a Pd(IPr) catalyst.

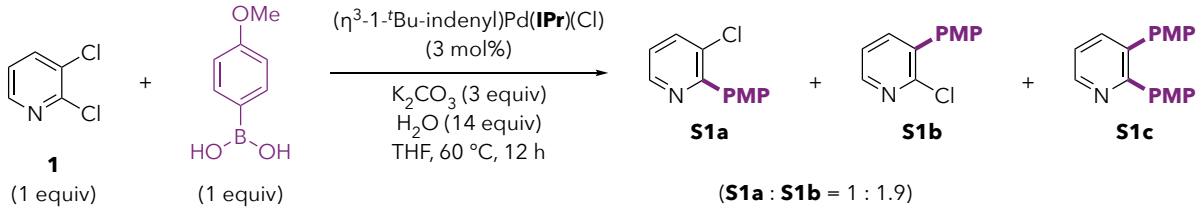

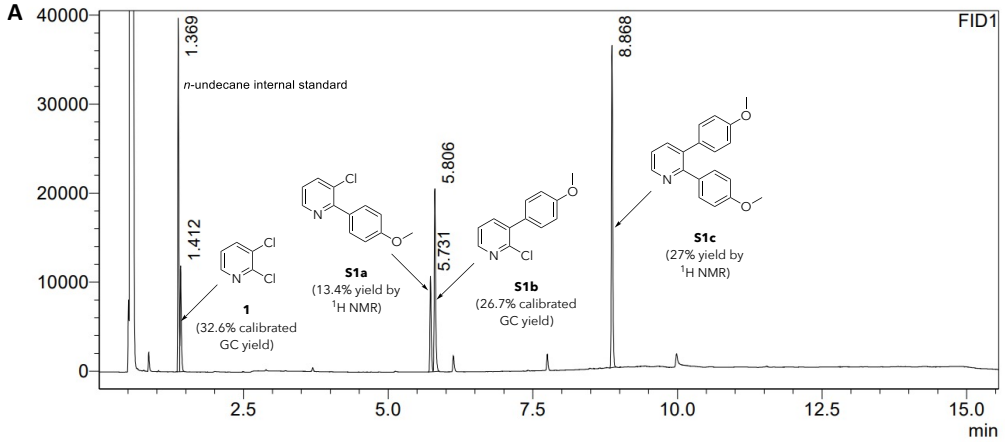

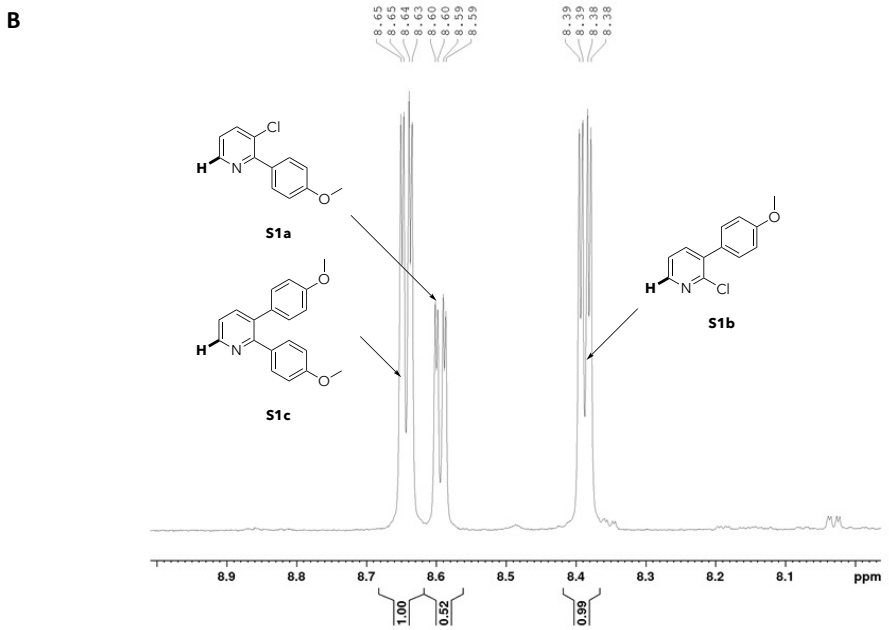

2,5-Dichloropyridine (**4**) favors reaction at C2 under the optimized system according to crude GC and GCMS analysis (ratio of **S4b** to **S4a** = 1 : 2.1 based on the ratio of signal integrations by ^{1}H-NMR ($CDCl_3$, 400 MHz, Scheme S4B). As such, the use of (η^3-1-^{t}Bu-indenyl)Pd(IPr)(Cl) does not enable unconventional selectivity with this substrate. As discussed in the manuscript, the difference in LUMO coefficient between C2 and C5 is very small (8% C2 and 10% C5), and thus it is likely that palladium is more strongly influenced by bond dissociation energies (which favor reaction at C2) than by LUMO coefficients.

Scheme S4. Suzuki reaction of **4** using a Pd(IPr) catalyst.

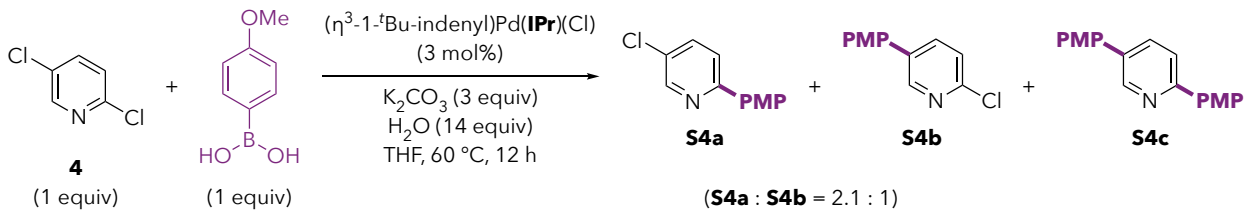

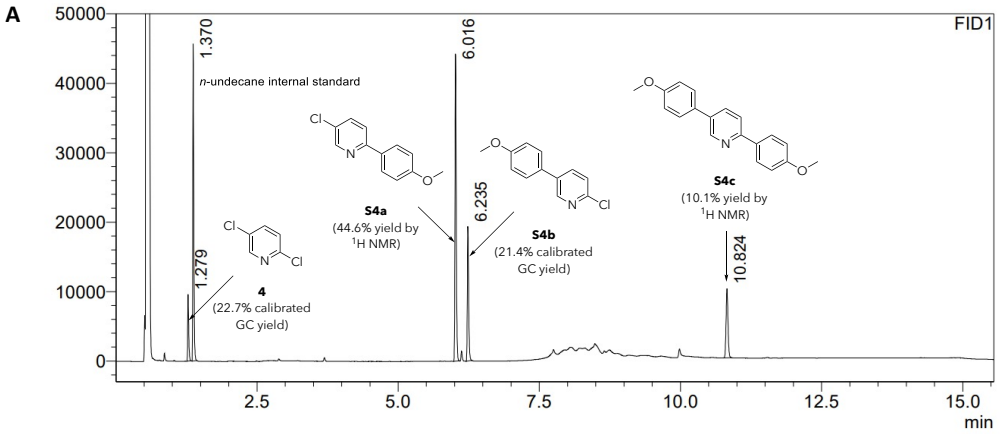

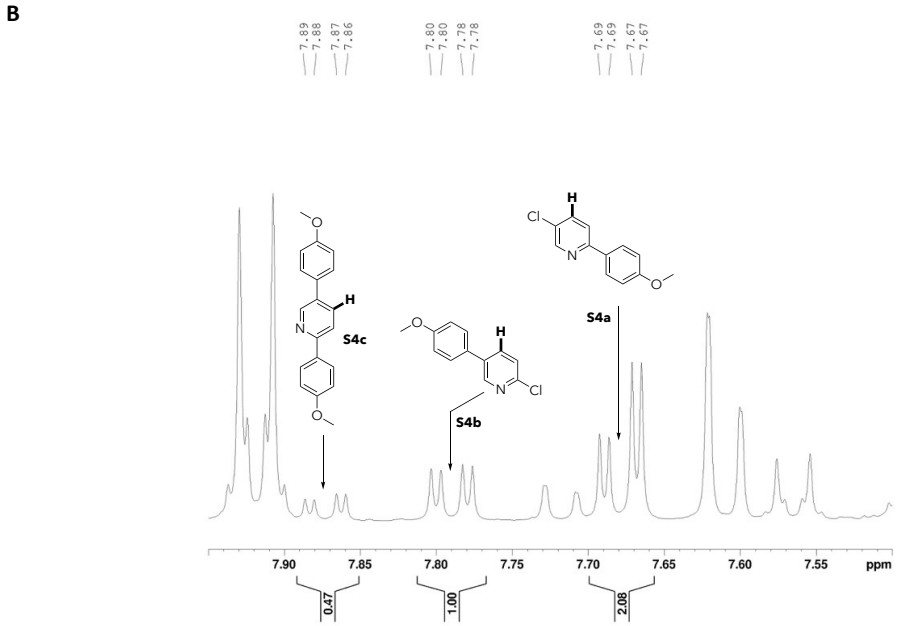

G. Isolation and Characterization of Cross-Coupled Products (Table 1 and Scheme 2)

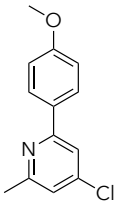

4-Chloro-2-(4-methoxyphenyl)-6-methylpyridine (15a). Compound **15a** was prepared according to a modified literature procedure.[6] Palladium(II) acetate (4.5 mg, 0.02 mmol, 5 mol %), 1,1'-bis(diphenylphosphino)ferrocene (14.8 mg, 0.2 mmol, 5 mol %), cesium carbonate (325.8 mg, 1 mmol 2.5 equiv) and *p*-methoxyphenylboronic acid (60.8 mg, 0.4 mmol, 1 equiv) were added to an oven-dried 1-dram vial in a N_2-filled glovebox. The vial was sealed with a septum, removed from the glovebox, and 2,4-dichloro-6-methylpyridine (**15**, 64.8 mg, 0.4 mmol, 1 equiv), deionized water (50 µL, 2.8 mmol, 7 equiv), and 1,4-dioxane (1.6 mL) were added through the septum. The reaction was allowed to stir at 70 °C for 21 h. Purification by flash column chromatography (R_f = 0.63 in 20% ethyl acetate in hexanes) provided a pure fraction of **15a** that was used for characterization and for preparing GC calibration curves. ^{1}H NMR (500 MHz, $CDCl_3$, δ): 7.91-7.95 (m, 2H), 7.46 (d, *J* = 1.4 Hz, 1H), 7.05 (d, *J* = 1.4 Hz, 1H), 6.96-7.01 (m, 2H), 3.86 (s, 3H), 2.58 (s, 3H). ^{13}C{^{1}H} NMR (126 MHz, $CDCl_3$, δ): 161.0, 159.9, 158.2, 144.7, 131.3, 128.6, 121.1, 117.3, 114.4, 55.6, 24.8. HRMS (ESI Q-TOF) m/z: [M]+ Calcd for $C_{13}H_{12}ClNO$ 233.0607; Found 233.0615.

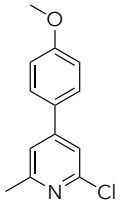

2-Chloro-4-(4-methoxyphenyl)-6-methylpyridine (15b). Compound **15b** was prepared according to the general procedure. An oven dried 1-dram vial was charged with a stir bar, (η^3-1-^{t}Bu-indenyl)Pd(IPr)Cl (8.4 mg, 0.012 mmol, 3.0 mol%), *p*-methoxyphenylboronic acid (60.8 mg, 0.4 mmol, 1 equiv), and potassium carbonate (165.8 mg, 1.2 mmol, 3 equiv). Dry degassed THF (1.6 mL), deionized water (100 µL, 5.6 mmol, 14 equiv), and 2,4-dichloro-6-methylpyridine (**15**, 64.8 mg, 0.4 mmol, 1 equiv) were added and the reaction mixture was sparged with N_2. The reaction was allowed to stir at 25 °C for 20 h. Purification was performed by reversed phase flash column chromatography with a 12 g C18 silica column, using an initial automated program comprising of a flow rate of 30 mL/min of water:acetonitrile (98:2 to 2:98) over 30 column volumes. When the product began eluting, the program was paused and reset to elute the analyte at 63% MeCN in water. After the elution, the initial program was resumed. Pure fractions containing **15b** were partitioned between dichloromethane and saturated brine. The organic layers were combined, dried over magnesium sulfate, and solvent was removed under reduced pressure affording a pure fraction of **15b** that was used for characterization and for preparing GC calibration curves. ^{1}H NMR (500 MHz, $CDCl_3$, δ): 7.52-7.59 (m, 2H), 7.31 (d, *J* = 0.8 Hz, 1H), 7.24 (d, *J* = 0.8, 1H), 6.97- 7.02 (m, 2H), 3.87 (s, 3H), 2.57 (s, 3H) ^{13}C{^{1}H} NMR (126 MHz, $CDCl_3$, δ): 161.0, 159.6, 151.4, 151.3, 129.5, 128.4, 119.5, 118.5, 114.7, 55.6, 24.4. HRMS (ESI Q-TOF) m/z: [M]+ Calcd for $C_{13}H_{12}ClNO$ 233.0607; Found 233.0643.

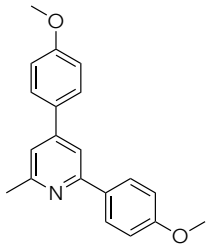

2,4-Bis(4-methoxyphenyl)-6-methylpyridine (15c). Compound **15c** was prepared according to a modified literature procedure.[1] An oven dried 1-dram vial was charged with a stirbar, (η^3-1-^{t}Bu-indenyl)Pd(IPent)Cl (9.8 mg, 0.012 mmol, 3.0 mol%), *p*-methoxyphenylboronic acid (121.6 mg, 0.8 mmol, 2 equiv), and potassium carbonate (165.8 mg, 1.2 mmol, 3 equiv). Benzene (1.6 mL), water (100 µL, 5.6 mmol, 14 equiv), and 2,4-dichloro-6-methylpyridine (**15**, 64.8 mg, 0.4 mmol, 1 equiv) was added quickly and the vial was sparged with N_2. The reaction was allowed to stir at 25 °C for 20 h. Purification by flash column chromatography (R_f = 0.29 in 20% ethyl acetate in hexanes) afforded **15c** as a white solid (86.6 mg, 64% yield). ^{1}H NMR (500 MHz, $CDCl_3$, δ): 8.02-7.97 (m, 2H), 7.64–7.58 (multiple peaks, 3H), 7.21 (d, *J* = 1.2 Hz, 1H), 7.03-6.99 (m, 4H), 3.88 (s, 3H), 3.87 (s, 3H), 2.66 (s, 3H). Spectral data are consistent with those previously reported.[7]

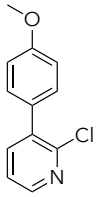

2-Chloro-3-(4-methoxyphenyl)pyridine (S1b). Compound **S1b** was prepared according to the general procedure. An oven dried 1-dram vial was charged with a stir bar, (η^3-1-^{t}Bu-indenyl)Pd(IPr)Cl (8.4 mg, 0.012 mmol, 3.0 mol%), 2,3-dichloropyridine (**1**, 59.2 mg, 0.4 mmol, 1.0 equiv), *p*-methoxyphenylboronic acid (60.8 mg, 0.4 mmol, 1.0 equiv), and potassium carbonate (165.8 mg, 1.2 mmol, 3 equiv). Benzene (1.6 mL) and water (100 µL, 5.6 mmol, 14 equiv) were added and the reaction was allowed to stir for 16 h. Purification by flash column chromatography on silica (R_f = 0.42 in 20% ethyl acetate in hexanes) provided **S1b** as white solid (21.9 mg, 25% yield). ^{1}H NMR (400 MHz, $CDCl_3$, δ): 8.36 (dd, *J* = 4.8, 1.9 Hz, 1H), 7.65 (dd, *J* = 7.6, 1.9 Hz, 1H), 7.41-7.37 (m, 2H), 7.29 (dd, *J* = 7.6, 4.8 Hz, 1H), 7.01-6.96 (m, 2H), 3.86 (s, 3H). ^{13}C{^{1}H} NMR (101 MHz, $CDCl_3$, δ): 159.8, 150.0, 148.2, 139.8, 136.9, 130.7, 130.0, 122.7, 114.0, 55.5. HRMS (ESI Q-TOF) m/z: [M]+ Calcd for $C_{12}H_{10}ClNO$ 219.0451; Found 219.0454. The other regioisomer (the C2 monoarylated isomer **S1a**) has been previously reported,[8] and its spectral data are distinct from those of product **S1b** reported here.

H. Time Trial for Suzuki Reaction of 2

The Pd/IPr-mediated coupling of 2,4-dichloropyridine and *p*-methoxyphenyl boronic acid was monitored over a period of 155 min. Two identical reactions were set up in parallel according to the General Procedure for GC-scale reactions using 1-dram reaction vials with the following modifications. Each reaction was run on a 0.6 mmol scale with respect to the limiting reagents (2,4-dichloropyridine and *p*-methoxyphenylboronic acid). One vial was designated as a "control" (sealed with a PTFE-lined cap, no aliquots removed), and the other was equipped with a septum cap. An *n*-undecane internal standard was added to both vials prior to stirring and both were sparged with N_2 prior to stirring. Aliquots were withdrawn from the second vial by syringe, diluted in ethyl acetate, and analyzed quantitatively by GC. The final aliquot at t = 155 min gave results comparable to the control vial (entries 5-6 in Table S9), demonstrating that the periodic removal of aliquots did not significantly alter the course of the reaction.

Table S9. Product Formation Over Time Using the Pd/IPr Conditions for the Suzuki Coupling of **1**.

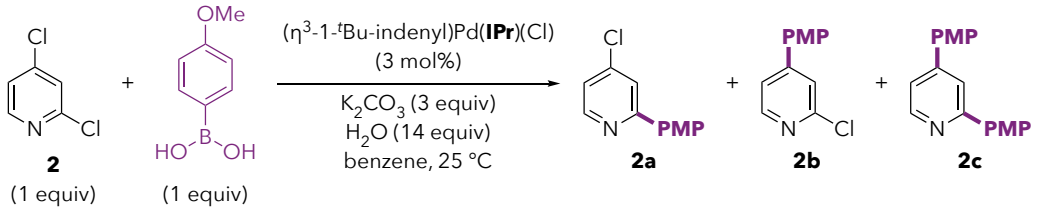

entry	time (min)	**2** (%)	**2a** (%)	**2b** (%)	**2c** (%)	**2a** : **2b**
1	5	93	trace	3	2	--
2	15	80	2	12	4	1 : 6
3	35	53	5	37	4	1 : 8
4	75	26	8	63	6	1 : 8
5	155	16	9	75	8	1 : 8
6	155 (control)	15	9	75	8	1 : 8

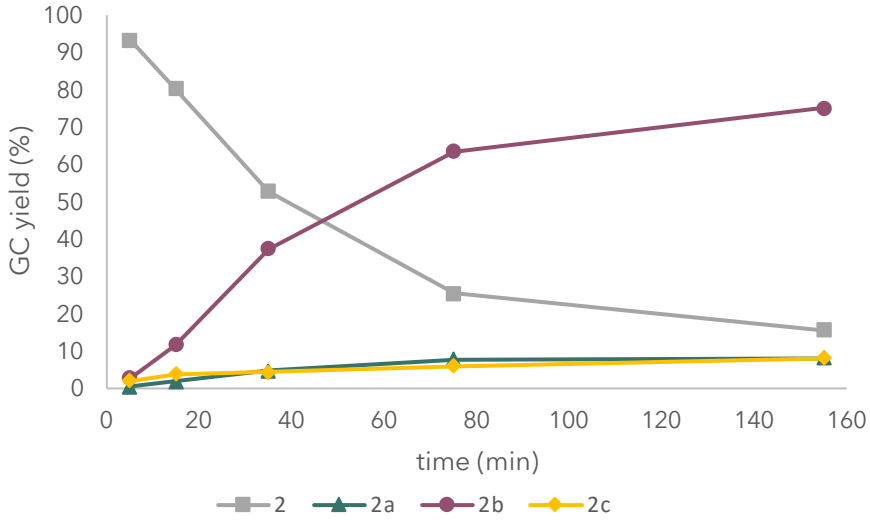

Figure S1. Visual representation of product formation over time using Pd/IPr conditions for the Suzuki coupling of **2**.

Discussion: C4 over C2-selectivity remains constant after the first 15 minutes (Table S9 and Figure S1). The C2-monoarylated isomer **2a** might be somewhat more likely to undergo a second arylation than the C4-monoarylated isomer **2b** when a 1:1 ratio of electrophile and nucleophile is used. Both chloride and arylated pyridines (potential ligands for Pd) build up throughout the reaction, yet these factors are not expected to improve C4-selectivity based on our mechanistic understanding of selectivity. Although aliquot removal may alter the ratio of homogeneous to heterogeneous material within the reaction vial, the control vial closely resembles the second vial after 155 min indicating that this effect was not significant.

I. *Evidence Against Multinuclear Speciation*

1. Effect of Pd:L ratio

Fairlamb et al. recently found that the selectivity of Pd/PPh_3-catalyzed cross-coupling of 2,4-dibromopyridine is sensitive to the ratio of Pd:PPh_3.[9] This was interpreted as a change in catalyst speciation depending on the amount of ligand [i.e., predominantly mononuclear Pd at high [PPh_3] (2-4 equiv relative to Pd) and multinuclear Pd at low [PPh_3] (<2 equiv relative to Pd)]. Fairlamb's results are summarized below (ratios approximated from Figure 1 of ref 9a). To highlight the significant effect of stoichiometry in Fairlamb's system, the differences in free energies of activation are also listed below. This value ($\Delta\Delta G^{\ddagger}$) represents the difference in the free energy barrier for reaction at C4 vs. C2 based on the reported experimental selectivity, and derived with the Eyring equation at 40 °C (Fairlamb's reaction temperature).

Table S10. Influence of Pd:L Ratio on Selectivity in Fairlamb's System[a]

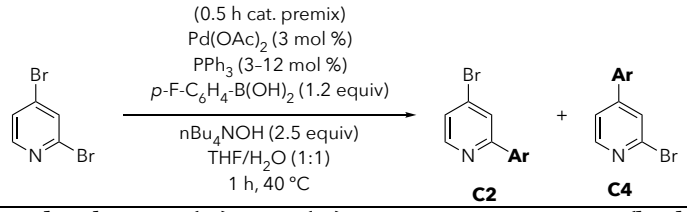

entry	Pd:PPh_3	**C2** (%)	**C4** (%)	**C2 : C4**	$\Delta\Delta G^{\ddagger}_{(C4-C2)}$ (kcal/mol)[b]
1	1 : 1	6	79	1 : 13	-1.6
2	1 : 1.5	8	78	1 : 9.8	-1.4
3	1 : 2	10	76	1 : 7.6	-1.3
4	1 : 2.5	7	24	1 : 3.4	-0.8
5	1 : 4	10	5	2 : 1	+0.4

[a]Product yields are estimated from Figure 1 of ref 9a. [b]Difference in free energies of activation for reaction at C4 versus C2 calculated from the estimated experimental product ratios using the Eyring equation at 313.15 K.

In contrast, we observe a negligible effect of metal to ligand ratio when additional free IPr or IMes is added to the reactions with (η^3-1-^{t}Bu-indenyl)Pd(NHC)(Cl). In contrast to Fairlamb's system, the results in our system suggest that there is not a catalyst speciation change upon changing ligand quantity.

Table S11. Influence of Pd:L Ratio on Selectivity in Our System with L = IPr[a]

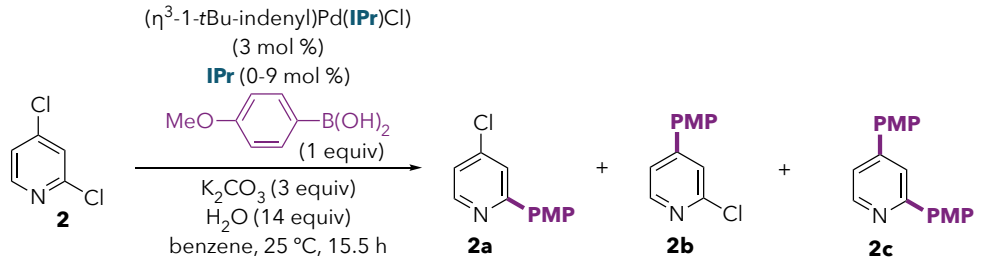

entry	trial	Added IPr (mol %)	Pd:IPr	**2a** (%)	**2b** (%)	**2c** (%)	**2a : 2b**	$\Delta\Delta G^{\ddagger}_{(C4-C2)}$ (kcal/mol)[b]
1	1	0	1 : 1	8.1	69	6	1 : 8.1	-1.2
2	2	0	1 : 1	8.6	70.5	6.4	1 : 8.6	-1.3
3	Average	0	1 : 1	8.4	69.8	6.2	1 : 8.3	-1.3

4	1	1.5	1 : 1.5	7.9	77.3	6.8	1 : 9.7	-1.3
5	2	1.5	1 : 1.5	7.6	70.9	6.6	1 : 9.3	-1.3
6	Average	1.5	1 : 1.5	7.8	74.1	6.7	1 : 9.5	-1.3
7	1	3.0	1 : 2	7.9	75.3	8.8	1 : 9.6	-1.3
8	2	3.0	1 : 2	8.0	74.5	5.7	1 : 9.3	-1.3
9	Average	3.0	1 : 2	8.0	74.9	7.2	1 : 9.4	-1.3
10	1	4.5	1 : 2.5	8.0	77.8	4.3	1 : 9.7	-1.3
11	2	4.5	1 : 2.5	8.5	79.4	4.1	1 : 9.3	-1.3
12	Average	4.5	1 : 2.5	8.3	78.6	4.2	1 : 9.5	-1.3
13	1	9.0	1 : 4	8.4	79.8	4.0	1 : 9.5	-1.3
14	2	9.0	1 : 4	8.6	78.7	4.9	1 : 9.1	-1.3
15	Average	9.0	1 : 4	8.5	79.3	4.5	1 : 9.3	-1.3

[a]Reactions were conducted according to the General Procedure for GC-scale reactions. GC yields calibrated against undecane as an internal standard. [b]Difference in free energies of activation for reaction at C4 versus C2 calculated from the experimental product ratios using the Eyring equation at 298.15 K.

Table S12. Influence of Pd:L Ratio on Selectivity in Our System with L = IMes[a]

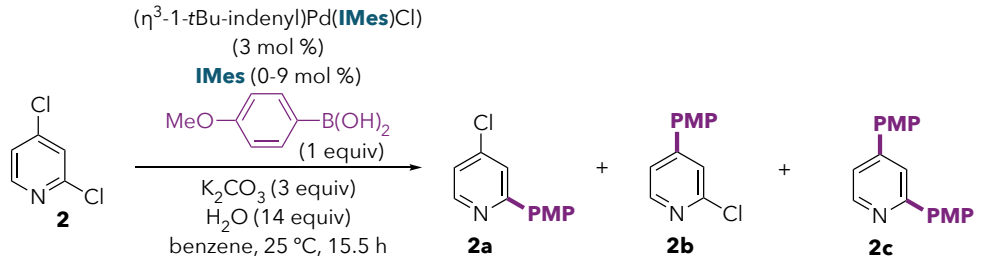

entry	trial	Added IMes (mol %)	Pd:IMes	**2a** (%)	**2b** (%)	**2c** (%)	**2a** : **2b**	$\Delta\Delta G^{\ddagger}_{(C4\text{-}C2)}$ (kcal/mol)[b]
1	1	0	1 : 1	21.1	35.3	2.7	1 : 1.7	-0.3
2	2	0	1 : 1	24.3	44.0	3.0	1 : 1.8	-0.3
3	Average	0	1 : 1	22.7	39.7	2.9	1 : 1.7	-0.3
4	1	1.5	1 : 1.5	26.3	54.0	4.9	1 : 2.1	-0.4
5	2	1.5	1 : 1.5	26.5	55.5	5.6	1 : 2.1	-0.4
6	Average	1.5	1 : 1.5	26.4	54.8	5.3	1 : 2.1	-0.4
7	1	3.0	1 : 2	27.1	55.0	5.0	1 : 2.0	-0.4
8	2	3.0	1 : 2	28.8	55.9	5.1	1 : 1.9	-0.4
9	Average	3.0	1 : 2	28.0	55.5	5.1	1 : 2.0	-0.4
10	1	4.5	1 : 2.5	26.6	54.3	3.8	1 : 2.0	-0.4
11	2	4.5	1 : 2.5	28.9	54.0	3.5	1 : 1.9	-0.4
12	Average	4.5	1 : 2.5	27.8	54.2	3.7	1 : 1.9	-0.4
13	1	9.0	1 : 4	24.8	48.4	2.5	1 : 2.0	-0.4
14	2	9.0	1 : 4	27.7	50.4	1.7	1 : 1.8	-0.3
15	Average	9.0	1 : 4	26.2	49.4	2.1	1 : 1.9	-0.4

[a]Reactions were conducted according to the General Procedure for GC-scale reactions. GC yields calibrated against undecane as an internal standard. [b]Difference in free energies of activation for reaction at C4 versus C2 calculated from the experimental product ratios using the Eyring equation at 298.15 K.

2. Effect of [Pd]

The effect of catalyst loading on the selectivity of the Suzuki coupling using (η^3-1-*t*Bu-indenyl)Pd(IPr)(Cl) and (η^3-1-*t*Bu-indenyl)Pd(IMes)(Cl) was evaluated. If multinuclear species are involved in the C4-selective pathway, then changes in selectivity would be expected upon changing initial precatalyst concentration, since multinuclear

species would form more rapidly at higher [Pd]. However, using (η^3-1-^{t}Bu-indenyl)Pd(IPr)(Cl), selectivity remains essentially constant from 0.5–10 mol % catalyst loading:

Table S13. Influence of [Pd] on Selectivity using IPr[a]

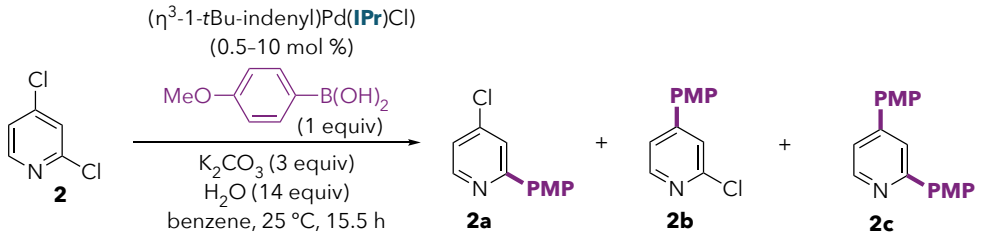

entry	trial	Pd mol %	**2a** (%)	**2b** (%)	**2c** (%)	**2a** : **2b**	$\Delta\Delta G^{\ddagger}_{(C4\text{-}C2)}$ (kcal/mol)[b]
1	1	0.5	4.2	32.9	1.1	1 : 7.8	
2	2	0.5	5.0	40.6	1.8	1 : 8.1	
3	Average	0.5	4.6	36.8	1.5	1 : 8.0	-1.2
4	1	1	4.4	36.0	1.5	1 : 8.2	
5	2	1	5.6	46.5	3.0	1 : 8.3	
6	Average	1	5.0	41.3	2.3	1 : 8.3	-1.3
7	1	3	8.1	69.0	6.0	1 : 8.5	
8	2	3	8.6	70.5	6.4	1 : 8.2	
9	Average	3	8.3	69.7	6.2	1 : 8.4	-1.3
10	1	5	8.6	69.9	4.3	1 : 8.1	
11	2	5	8.5	71.7	5.3	1 : 8.4	
12	Average	5	8.6	70.8	4.8	1 : 8.2	-1.2
13	1	10	8.0	67.4	3.8	1 : 8.4	
14	2	10	8.2	71.3	5.0	1 : 8.7	
15	Average	10	8.1	69.4	4.4	1 : 8.6	-1.3

[a]Reactions were conducted according to the General Procedure for GC-scale reactions. GC yields calibrated against undecane as an internal standard. [b]Difference in free energies of activation for reaction at C4 versus C2 calculated from the experimental product ratios using the Eyring equation at 298.15 K.

With (η^3-1-^{t}Bu-indenyl)Pd(IMes)(Cl) (below) the reaction is slightly less selective (more reaction at C2) at low catalyst loadings. This is consistent with our observation that, with Pd/IMes, more reaction at C2 is observed at higher 2,4-dichloropyridine concentration (*vide supra*). At lower catalyst loadings, the effective substrate:Pd concentration is higher, which can explain the slight influence of catalyst loading on selectivity.

Table S14. Influence of [Pd] on Selectivity using IMes[a]

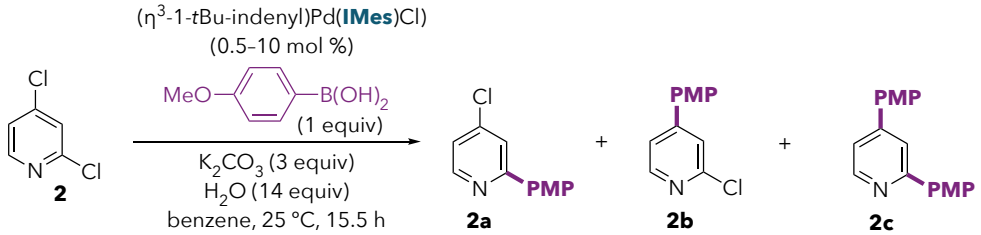

entry	trial	Pd mol %	**2a** (%)	**2b** (%)	**2c** (%)	**2a** : **2b**	$\Delta\Delta G^{\ddagger}_{(C4\text{-}C2)}$ (kcal/mol)[b]
1	1	0.5	4.7	5.7	0.3	1 : 1.2	
2	2	0.5	4.4	5.9	0.2	1 : 1.3	
3	Average	0.5	4.6	5.8	0.3	1 : 1.3	-0.1
4	1	1	6.0	8.3	0.3	1 : 1.4	
5	2	1	10.1	14.0	0.4	1 : 1.4	
6	Average	1	8.1	11.2	0.4	1 : 1.4	-0.2
7	1	3	21.1	35.3	2.7	1 : 1.7	
8	2	3	24.3	44.0	3.0	1 : 1.8	
9	Average	3	22.7	39.6	2.9	1 : 1.7	-0.3
10	1	5	25.3	43.5	2.4	1 : 1.7	
11	2	5	29.2	48.7	3.3	1 : 1.7	
12	Average	5	27.3	46.1	2.9	1 : 1.7	-0.3
13	1	10	26.1	40.2	2.5	1 : 1.5	
14	2	10	24.5	43.4	2.5	1 : 1.8	
15	Average	10	25.3	41.8	2.5	1 : 1.7	-0.3

[a]Reactions were conducted according to the General Procedure for GC-scale reactions. GC yields calibrated against undecane as an internal standard. [b]Difference in free energies of activation for reaction at C4 versus C2 calculated from the experimental product ratios using the Eyring equation at 298.15 K.

3. Comments on Reaction Color

Under the standard conditions for C4-selective coupling catalyzed by (η^3-1-^{t}Bu-indenyl)Pd(NHC)(Cl), there is no visual indication of nanoparticle formation. Whereas reactions are reported to turn dark brown/black under Fairlamb's conditions[9] and under our previously reported ligand-free "Jeffery" conditions,[1] the reactions using (η^3-1-^{t}Bu-indenyl)Pd(NHC)(Cl) remain pale yellow throughout the duration of the experiment, as illustrated below:

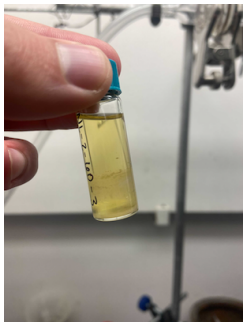

Figure S2. Reactions catalyzed by (η^3-1-^{t}Bu-indenyl)Pd(NHC)(Cl) remain pale yellow, giving no indication of nanoparticle formation.

II. Computational Details

A. General Methods

Calculations were performed with Gaussian 16.[10] An ultrafine integration grid and the keyword 5d were used for all calculations. Geometry optimizations of stationary points were carried out in implicit solvent using the CPCM continuum solvation model[11] (THF) with MN15L,[12] LANL2DZ[13] for Pd, and 6-31+G(d) for all other atoms ("BS1"). Frequency analyses were carried out at the same level to evaluate the zero-point vibrational energy and thermal corrections at 298.15 K. The nature of the stationary points was determined in each case according to the appropriate number of negative eigenvalues of the Hessian matrix. Forward and reverse intrinsic reaction coordinate (IRC) calculations were carried out on the optimized transition structures to ensure that the TSs indeed connect the appropriate reactants and products.[14] Multiple conformations were considered for all structures, and the lowest energy conformations are reported. It is worth noting that the lowest-energy π-complexes are not necessarily directly connected to the oxidative addition transition structures on the potential energy surfaces (i.e., in some cases the IRC calculations, in particular for reaction at C2, lead to different higher-energy π complexes than the lowest-energy structures reported). This factor is unimportant to the overall energetics, assuming that the barrier to interconverting π-complexes is low (e.g., by palladium ring-walking). Unless otherwise indicated, the final reported energies were obtained from single point energy calculations on the optimized geometries using MN15,[15] the CPCM solvation model (THF), and a larger basis set (SDD[16] for Pd and 6-311++G(2d,p) for all other atoms, "BS2"). Gibbs free energy values are reported after applying Cramer and Truhlar's anharmonic correction to frequencies that are less than 100 cm^{-1}.[17] All thermodynamic quantities were computed with the GoodVibes code[18] at 298.15 K, applying corrections for initial concentrations consistent with the optimized experimental conditions ([Pd] = 0.0075 *M* and [**2**] = 0.25 *M*). 3D images of optimized structures were generated with CYLview.[19] 3D images of molecular orbitals were generated with Avogadro.[20]

B. Benchmarking Calculations and Method-Dependence of TS13a-IMes Energetics

1. Geometry Optimizations

The functional used for geometry optimizations (MN15L) was selected for several reasons. First, benchmarking calculations performed on (η^3-1-^{t}Bu-indenyl)Pd(NHC)(Cl) showed that, out of four functionals (MN15L, M06, B3LYP, and B3LYP-D3BJ), MN15L gave the lowest root mean square deviation (RMSD) for several key bond distances when compared to the published crystal structure.[21]

Table S15. MN15L gives the lowest error in bond distances when compared to a crystal structure.

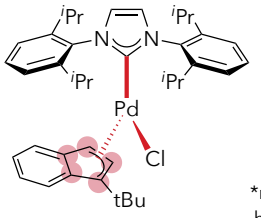

functional	RMSD*
MN15L	0.10
M06	0.15
B3LYP	0.35
B3LYP-D3BJ	0.27

*root mean squared error for the 7 distances highlighted in red (includes Pd–C distances for each of the carbons of the 5-membered ring)

Furthermore, recent benchmarking studies on the performance of DFT functionals for computing bond energies of 3d transition metals concluded that "*...Overall, the best performing functionals are PW6B95, the MN15 and MN15-L functionals, and the double hybrid B2PLYP*."[22]

Finally, in recent work on related systems (oxidative addition of chloroaryl triflates at $Pd(0)L_n$), we found that MN15L gave the best correlation to experiment.[23] Based on all of these considerations, MN15L was chosen as the functional for geometry optimizations.

2. Single Point Energy Calculations

In choosing a functional for single-point energy calculations using a larger basis set, we first compared the predicted selectivity of Pd-IPr using 4 different functionals for single point energy calculations (MN15L, MN15, M06, and B3LYP-D3). All 4 functionals led to similar predictions (Table S16).

Table S16. Effect of Functional on Predicted C2:C4 Selectivity with Pd(IPr)

functional	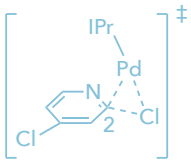 **TS10a-IPr**	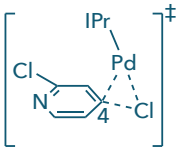 **TS10b-IPr**	$\Delta\Delta G^{\ddagger}_{(\mathbf{TS10b\text{-}TS10a})}$	predicted C2 : C4
MN15L	11.5	10.4	-1.1	1 : 6
MN15	13.8	12.1	-1.7	1 : 17
M06	10.0	8.7	-1.3	1 : 9
B3LYP-D3BJ	8.6	7.9	-0.7	1 : 3

ΔG‡ values in kcal/mol, measured from preceding pi complex. Calculations at the [functional]/6-311++G(2d,p)/SDD(Pd) // MN15L/6-31+G(d)/LANL2DZ(Pd) level of theory.

We next evaluated several functionals for single point energy calculations on the lowest-energy TSs for reaction at C4 (monoligated, **TS10b-IMes**) and at C2 (bisligated, **TS13a-IMes**) using the ligand IMes. The numbers below are adjusted for initial concentration. Although the single point energy functional does not seem to matter very much when comparing **TS10a-IPr** and **TS10b-IPr** (Table S16 above), the relative energies of **TS10b-IMes** and **TS13a-IMes** were found to vary enormously with functional (Table S17). This is likely due to the crowdedness of **TS13a-IMes** and differences in how the functionals handle dispersion interactions.

Table S17. Effect of Functional on Predicted C2:C4 Selectivity with Pd(IMes)

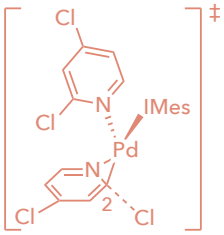

TS13a-IMes

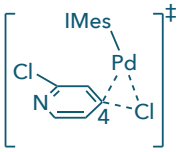

TS10b-IMes

functional	$\Delta\Delta G^{\ddagger}_{(\textbf{TS10b-TS13a})}$	predicted C2 : C4
MN15L	+3.5	368 : 1
MN15	+1.4	11 : 1
M06L	+3.7	516 : 1
M06	-4.2	1 : 1,199
B3LYP-D3BJ	+7.1	160,277 : 1
wB97XD	+3.6	436 : 1

ΔΔG‡ values in kcal/mol. Calculations at the [functional]/6-311++G(2d,p)/SDD(Pd) // MN15L/6-31+G(d)/LANL2DZ(Pd) level of theory.

As shown above, most functionals predict that, with IMes, the C2 product should be favored, although the predicted selectivities with those functionals span 5 orders of magnitude. On the other hand, M06 predicts that the C4 product should be exclusively observed. Overall, the selectivity predicted with the hybrid functional MN15 provides results that are most consistent with the near 1:1 selectivity observed experimentally.

We next further evaluated some of these functionals in another crowded system where dispersion interactions would also be important. The energies of the minimum-energy transition structures for reaction at C2 and C4 with $Pd(PPh_3)_2$ were calculated (Table S18). Experimentally, the use of PPh_3 leads exclusively to the C2-functionalized product. As shown below, both MN15 and M06 provide predictions consistent with experiment for this system. However, MN15L fails to predict the very high experimental selectivity (predicted C2:C4 ~ 13:1, experimental >99:1).

Table S18. Effect of Functional on Predicted C2:C4 Selectivity with $Pd(PPh_3)_2$.

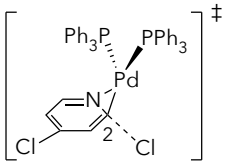

C2

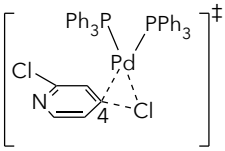

C4

functional	$\Delta\Delta G^{\ddagger}_{(\textbf{C4-C2})}$	predicted C2 : C4
MN15L	+1.5	13 : 1
MN15	+5.0	4,628 : 1
M06	+4.2	1,199 : 1

ΔΔG‡ values in kcal/mol. Calculations at the [functional]/6-311++G(2d,p)/SDD(Pd) // MN15L/6-31+G(d)/LANL2DZ(Pd) level of theory.

Notably, MN15 and MN15L give identical predictions for selectivity with $Pd(PMe_3)_2$, a much smaller system in which dispersion interactions are significantly less important (Table S19). The predicted ratio of C2:C4 = 3:1 is similar to the experimentally observed selectivity of ~11:1.

Table S19. Effect of Functional on Predicted C2:C4 Selectivity with $Pd(PMe_3)_2$.

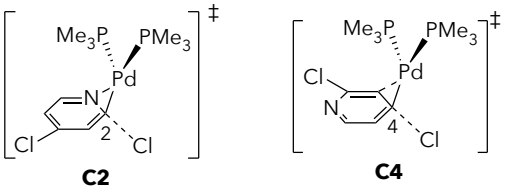

functional	$\Delta\Delta G^{\ddagger}_{(\mathbf{C4-C2})}$	predicted C2 : C4
MN15L	+0.6	3 : 1
MN15	+0.6	3 : 1

ΔΔG‡ values in kcal/mol. Calculations at the [functional]/6-311++G(2d,p)/SDD(Pd) // MN15L/6-31+G(d)/LANL2DZ(Pd) level of theory.

Based on all of these benchmarking calculations, MN15 was chosen for the single point energy calculations in this manuscript, and is expected to provide the best accuracy especially when comparing structures with very different degrees of crowdedness.

C. Frontier Molecular Orbital Calculations (Figure 1, Figure 2, Scheme 2B)

MO calculations were performed at the CPCM(THF)-MN15L/BS1 level of theory using the "pop=regular" keyword. The percent contribution of individual atoms to a given molecular orbital was calculated from the molecular orbital coefficients provided in the Gaussian output file. For a given MO, the absolute values of the coefficients for each atomic orbital of the carbon in question were summed. This sum was divided by the sum of the absolute values of the coefficients for each atomic orbital of all atoms in the molecule, and the result was multiplied by 100% to arrive at the %contribution of an individual carbon to that MO.

Graphical depictions of the LUMOs of **1**, **2**, **4**, and **5** from Scheme 2B are provided in Figure S3 below. Figure S4 illustrates the HOMOs of monoligated Pd(IPr) and bisligated Pd(IPr)(2,4-dichloropyridine). The latter is distorted into the bent geometry that it adopts during oxidative addition (structure was obtained from **TS13b-IPr**). Analogous to the simple model complexes $Pd(PMe_3)$ and $Pd(PMe_3)_2$, the HOMO of monoligated Pd(IPr) has σ-symmetry while the HOMO of bisligated Pd(IPr)(2,4-dichloropyridine) has π-symmetry.

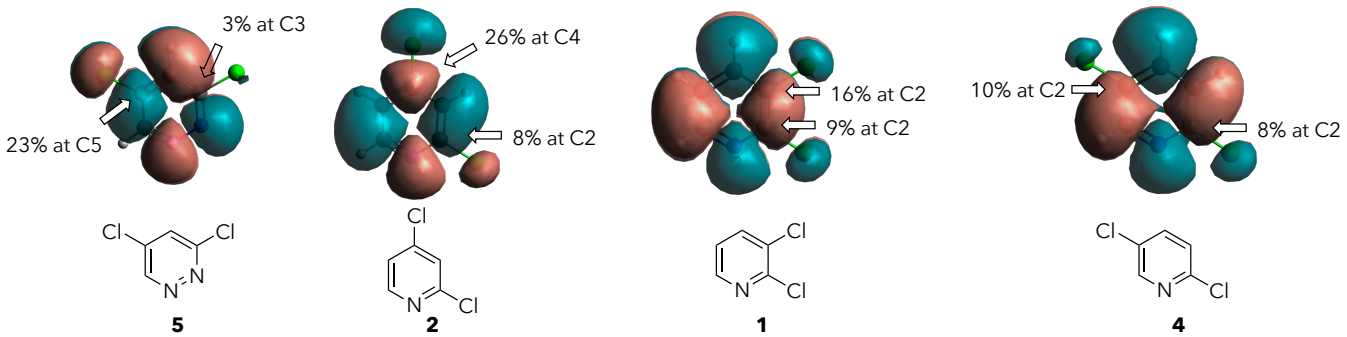

Figure S3. LUMOs of dichloroheteroarene substrates from Figure 2.

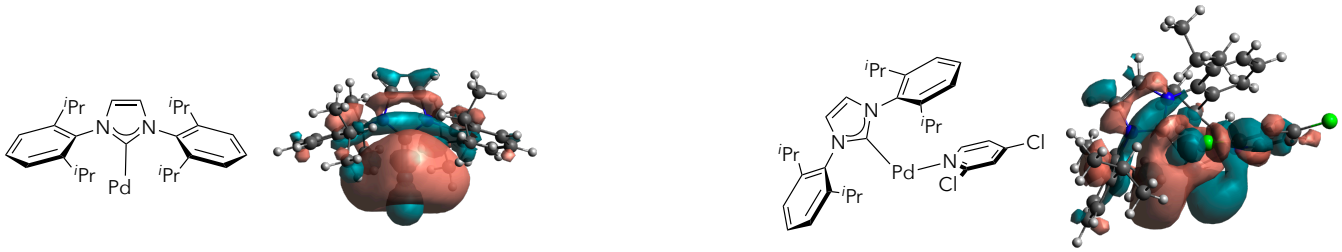

Figure S4. HOMOs of mono and bisligated Pd(IPr) complexes.

D. Higher Energy Transition Structures with Pd/IPr

With monoligated Pd(IPr), only 3-centered mechanisms were located for oxidative addition at C4 of **1** (**TS10b-IPr**). Three different conformations were found, and the lowest energy one is reported in the manuscript. Attempts to find displacement mechanisms were unsuccessful, as the geometries optimized to 3-centered concerted structures instead. For reaction at C2, three different conformations of a 3-centered mechanism were located, and the lowest energy one is reported in the manuscript (**TS10a-IPr**). In addition, one structure representing a displacement-type mechanism was found (**STS10a2-IPr**, below). Its energy is higher than any of the conformations of the 3-centered mechanism ($\Delta G^{\ddagger}$ = 17.8 kcal/mol relative to pi complex **9-IPr**). Seven conformations of bisligated transition structures were located each for reaction at both C2 and C4, and the lowest energy conformation for reaction at each site is reported in the manuscript (**TS13a-IPr** and **TS13b-IPr**). All of the bisligated conformations represent displacement mechanisms, and no 3-centered concerted structures could be found at the level of theory used in this work.

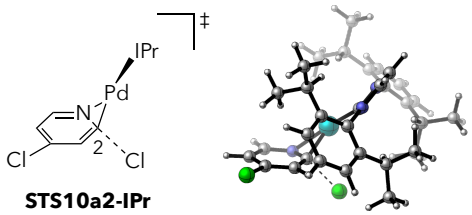

Figure S5. Structure of a higher-energy nucleophilic displacement mechanism for oxidative addition of C2-Cl at monoligated Pd(IPr).

E. Higher Energy Pd(0) Structures with IPr and IMes

As shown below, the lowest calculated coordination mode for Pd(0)(NHC) is the pre-oxidative addition pi complex.

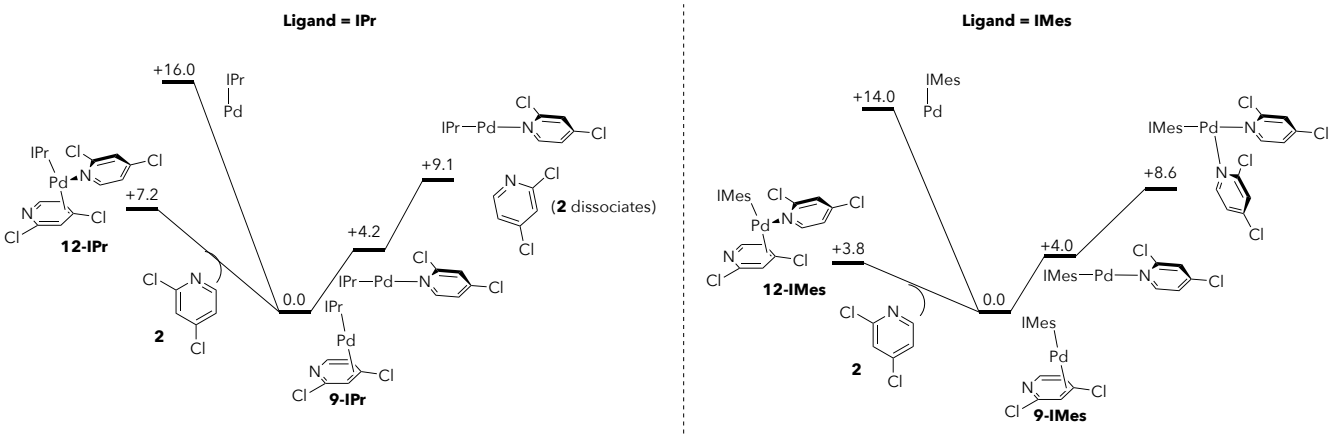

Figure S6. Other coordination environments for Pd(NHC) are higher-energy than Pd(NHC)(η^2-**2**).

F. Discussion About Selectivity-Influencing Factors Beyond PdL vs. PdL₂

Although L_2Pd vs. LPd seems to be the critical determining factor between a C2 vs C4 preference, there are also more subtle factors that influence the magnitude of that preference. Additional calculations were completed with phosphine ligands involving oxidative addition at monoligated $Pd(PMe_3)$, $Pd(PMe_3)_2$, $Pd(PPh_3)$, $Pd(PPh_3)_2$, and $Pd(P^tBu_3)$. Reaction at PdL is unlikely for with PMe_3 and probably also PPh_3 (but see ref 24, in which monoligated $Pd(PPh_3)$ is implicated during oxidative addition of PhBr). However, our calculations on (hypothetical) PdL illustrate some interesting differences between triarylphosphines, trialkylphosphines, and *N*-heterocyclic carbene ligands.

The more nuanced factors that influence the magnitude of C2 vs C4 preference seem to include:

(1) The nucleophilicity of PdL. This is related to the sigma-donicity of L, and is somewhat correlated with the energy of the HOMO for PdL. As shown in the table below, the predicted C4 selectivity of PdL trends with its HOMO energy.

Table S20. Correlation between Calculated Selectivity of PdL and HOMO Energy.

PdL	calc. $\Delta\Delta G_{(C4-C2)}^{\ddagger}$ (considering only PdL, kcal/mol)[a]	calc. selectivity (considering only PdL, C2 : C4)[a]	exp. selectivity of PdL (C2 : C4)	HOMO (eV)
$Pd(PPh_3)$	+0.3	2 : 1	N/A[b]	-0.218[c]
$Pd(P^tBu_3)$	-0.9	1 : 5	1 : 2	-0.215
$Pd(PMe_3)$	-1.4	1 : 11	N/A[b]	-0.208
Pd(IPr)	-1.7	1 : 18	1 : 10	-0.207
Pd(IMes)	-2.3	1 : 49	N/A[b]	-0.206

[a]Calculations performed at the CPCM(THF)-MN15/6-311++G(2d,p)/SDD(Pd)//CPCM(THF)-MN15L-6-31+G(d)/LANL2DZ(Pd) level of theory. [b]Under experimental conditions, reaction most likely occurs partly or completely through a bisligated Pd species, so it is not possible to assess the experimental selectivity of monoligated PdL. [c]Geometry optimization of $Pd(PPh_3)$ failed to converge, so a single point energy calculation was performed on a $Pd(PPh_3)$ fragment taken from a $Pd(PPh_3)$(**2**) pi complex.

(2) Whether a concerted or displacement mechanism is favored at C4 for PdL_2. This seems to be related to both the sterics and the electronics of L, and is a topic of ongoing detailed research in our group. Maseras et al. have shown that the mechanism of oxidative addition of PhBr varies with ligand,[25] and similarly we have found that the lowest-energy mechanism of oxidative addition at C4—Cl of 2,4-dichloropyridine varies with ligand. For $Pd(PMe_3)_2$ and $Pd(PPh_3)_2$, a displacement mechanism is favored for reaction at C2—Cl. However, although $Pd(PMe_3)_2$ also favors a displacement mechanism at C4—Cl, $Pd(PPh_3)_2$ reacts through a concerted mechanism at this position. This mechanistic difference may explain the exceedingly high C2-selectivity of $Pd(PPh_3)_2$, although the reason for this mechanistic difference is still under investigation.

Table S21. Comparison of Preferred Mechanism for Oxidative Addition with PdL_2 (L = PMe_3 or PPh_3).

PdL_2	mechanism at C2	mechanism at C4	calc. $\Delta\Delta G_{(C4-C2)}^{\ddagger}$ (considering only PdL_2, kcal/mol)	calc. selectivity (considering only PdL_2, C2 : C4)	exp. selectivity of PdL_2 (C2 : C4)
$Pd(PMe_3)_2$	displacement	displacement	+0.6	3 : 1	11 : 1
$Pd(PPh_3)_2$	displacement	concerted	+5.0	436 : 1	>99 : 1

Calculations performed at the CPCM(THF)-MN15/6-311++G(2d,p)/SDD(Pd)//CPCM(THF)-MN15L-6 31+G(d)/LANL2DZ(Pd) level of theory.

The partial charges at Pd were computed for **TS13a-IPr** and **TS13b-IPr** at the CPCM(THF)-MN15/6-311++G(2d,p)/SDD(Pd) level of theory. Palladium is *less positive* during the SN-type mechanism at C2 (**TS13a-IPr**) compared to at C4 (**TS13b-IPr**). This is consistent with nitrogen being more effective than carbon at stabilizing the building positive charge at Pd, and suggests that the reason for conventional C2-selectivity is more complicated than a simple comparison of C2—Cl vs C4—Cl bond strengths. This observation is consistent with a recent report by Leitch et al., in which conventional selectivity was found to correlate with more positive electrostatic potentials at the *ipso* carbon and with more negative potentials at an *ortho* carbon.[26]

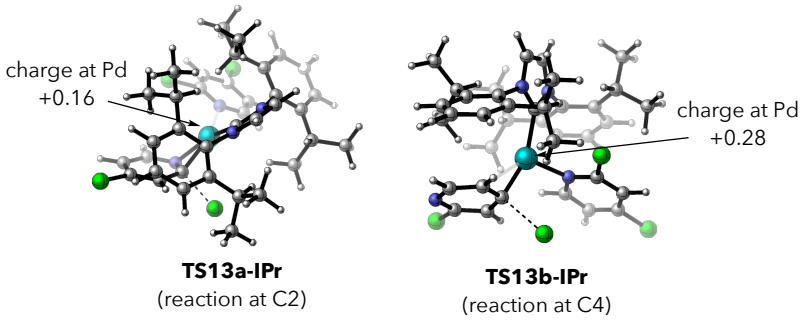

Figure S7. Partial charges at Pd during displacement-type oxidative addition at C2 versus C4 with Pd(IPr)(**2**).

G. Energies, Entropies, and Lowest Frequencies of Minimum Energy Structures

Table S22. Energies, Entropies, and Lowest Frequencies of Minimum Energy Structures[a]

Structure	E_{elec} (Hartree)	E_{elec} + ZPE (Hartree)	H (Hartree)	S (cal mol^{-1} K^{-1})	G[b] (Hartree)	$G_{corrected}$[c] (Hartree)	Lowest freq. (cm^{-1})	# of imag freq.
TS7a	-1280.102315	-1279.898129	-1279.881899	126.1	-1279.941812	-1279.939842	-181.5	1
TS7b	-1280.098858	-1279.894876	-1279.878312	130.7	-1279.940397	-1279.936888	-235.7	1
TS7c	-1280.084978	-1279.881161	-1279.864742	126.9	-1279.92503	-1279.923424	-221.5	1
TS8a	-1741.005607	-1740.687459	-1740.663099	163.3	-1740.740705	-1740.737083	-281.9	1
TS8b	-1741.011908	-1740.693341	-1740.669092	162.4	-1740.746256	-1740.743024	-201.9	1
2	-1167.119851	-1167.050102	-1167.042657	82.9	-1167.08032	-1167.08032	161.6	0
9-IPr	-2453.730783	-2453.090513	-2453.049859	236.9	-2453.164034	-2453.155668	17.7	0
TS10a-IPr	-2453.707733	-2453.068584	-2453.028051	238.4	-2453.142927	-2453.133659	-135.7	1
TS10b-IPr	-2453.710919	-2453.071466	-2453.031003	238.0	-2453.145702	-2453.13641	-67.2	1
11a-IPr	-2453.759276	-2453.117221	-2453.076806	235.8	-2453.19044	-2453.182122	18.6	0
11b-IPr	-2453.761652	-2453.119249	-2453.07897	234.4	-2453.191948	-2453.184179	20.7	0
12-IPr	-3620.866219	-3620.154355	-3620.106041	272.8	-3620.237269	-3620.226248	13.0	0
TS13a-IPr	-3620.849928	-3620.138432	-3620.090361	274.3	-3620.222277	-3620.210275	-210.2	1
TS13b-IPr	-3620.838787	-3620.127124	-3620.079188	268.4	-3620.208319	-3620.199264	-97.8	1
14a-IPr	-3620.887865	-3620.175356	-3620.126318	281.3	-3620.261591	-3620.247962	12.9	0
14b-IPr	-3620.893594	-3620.179807	-3620.131447	273.8	-3620.263159	-3620.252016	14.3	0
9-IMes	-2218.108449	-2217.641368	-2217.606774	218.2	-2217.712036	-2217.701551	15.6	0
TS10a-IMes	-2218.086513	-2217.61977	-2217.585916	211.1	-2217.687806	-2217.679412	-125.2	1
TS10b-IMes	-2218.090094	-2217.623379	-2217.589502	213.0	-2217.692295	-2217.683132	-69.1	1
11a-IMes	-2218.146487	-2217.677853	-2217.643676	212.7	-2217.746342	-2217.73791	15.1	0
11b-IMes	-2218.1467	-2217.678158	-2217.643855	214.0	-2217.747152	-2217.738397	18.1	0
12-IMes	-3385.24802	-3384.710021	-3384.667679	250.7	-3384.788405	-3384.777506	18.6	0
TS13a-IMes	-3385.236174	-3384.698285	-3384.656419	248.5	-3384.776068	-3384.76572	-219.3	1
TS13b-IMes	-3385.225136	-3384.686139	-3384.644748	243.6	-3384.762106	-3384.753188	-138.5	1
14a-IMes	-3385.299441	-3384.757995	-3384.71694	238.1	-3384.831658	-3384.824454	22.6	0
14b-IMes	-3385.279344	-3384.738809	-3384.697088	247.2	-3384.816127	-3384.805721	10.2	0
9-PtBu3	-2109.127974	-2108.686909	-2108.658464	177.2	-2108.744242	-2108.74063	25.2	0
TS10a-PtBu3	-2109.107486	-2108.666821	-2108.638888	175.0	-2108.723628	-2108.720074	-94.2	1
TS10b-PtBu3	-2109.109484	-2108.66843	-2108.640664	172.9	-2108.724422	-2108.721519	-34.0	1
11a-PtBu3	-2109.149996	-2108.707225	-2108.678913	176.0	-2108.764127	-2108.760791	22.1	0
11b-PtBu3	-2109.149804	-2108.705979	-2108.677991	174.0	-2108.762247	-2108.759133	31.5	0
12-PtBu3	-3276.258264	-3275.746426	-3275.709597	220.8	-3275.816112	-3275.807834	15.9	0
TS13a-PtBu3	-3276.236964	-3275.72466	-3275.688599	216.5	-3275.793088	-3275.785727	-218.9	1
TS13b-PtBu3	-3276.221176	-3275.709307	-3275.673113	216.2	-3275.77742	-3275.770766	-43.5	1
14a-PtBu3	-3276.282445	-3275.767875	-3275.731461	216.8	-3275.836078	-3275.829157	14.3	0
14b-PtBu3	-3276.280225	-3275.76592	-3275.72932	220.2	-3275.835525	-3275.827204	16.9	0

[a]Energy values calculated at the CPCM(THF)-MN15/BS2//CPCM(THF)-MN15L/BS1 level of theory. 1 Hartree = 627.51 kcal mol^{-1}. Thermal corrections at 298.15 K based on [Pd] = 0.0075 *M* and [**2**] = 0.25 *M*. [b]Solvent-corrected free energy given by G = E_{elec} + G_{corr}, where G_{corr} is the thermal correction to Gibbs free energy. [c]Solvent-corrected free energy given by G = E_{elec} + G_{corr*}, where G_{corr*} is the thermal correction to Gibbs free energy obtained after applying Cramer and Truhlar's anharmonic correction.[17]

III. References

1. Norman, J. P.; Larson, N. G.; Entz, E. D.; Neufeldt, S. R. Unconventional Site-Selectivity in Palladium-Catalyzed Cross-Couplings of Dichloroheteroarenes under Ligand-Controlled and Ligand-Free Systems. *J. Org. Chem.* **2022**, *87*, 7414-7421.

2. (a) Amatore, C.; Jutand, A.; M'Barki, M. A. Evidence of the Formation of Zerovalent Palladium from $Pd(OAc)_2$ and Triphenylphosphine. *Organometallics* **1992**, *11*, 3009-3013; (b) Amatore, C.; Carré, E.; Jutand, A.; M'Barki, M. A. Rates and Mechanism of the Formation of Zerovalent Palladium Complexes from Mixtures of Pd(OAc)2 and Tertiary Phosphines and Their Reactivity in Oxidative Additions. *Organometallics* **1995**, *14*, 1818-1826; (c) Wagschal, S.; Perego, L. A.; Simon, A.; Franco-Espejo, A.; Tocqueville, C.; Albaneze-Walker, J.; Jutand, A.; Grimaud, L. Formation of Xphos-Ligated Palladium(0) Complexes and Reactivity in Oxidative Additions. *Chem.-Eur. J.* **2019**, *25*, 6980-6987.

3. (a) Mitchell, E. A.; Jessop, P. G.; Baird, M. C. A Kinetics Study of the Oxidative Addition of Bromobenzene to $Pd(PCy_3)_2$ (Cy = cyclohexyl) in a Nonpolar Medium: The Influence on Rates of Added PCy_3 and Bromide Ion. *Organometallics* **2009**, *28*, 6732-6738; (b) Barrios-Landeros, F.; Carrow, B. P.; Hartwig, J. F. Effect of Ligand Steric Properties and Halide Identity on the Mechanism for Oxidative Addition of Haloarenes to Trialkylphosphine Pd(0) Complexes. *J. Am. Chem. Soc.* **2009**, *131*, 8141-8154; (c) McMullin, C. L.; Jover, J.; Harvey, J. N.; Fey, N. Accurate modelling of Pd(0) + PhX oxidative addition kinetics. *Dalton Trans.* **2010**, *39*, 10833-10836.

4. Gensch, T.; dos Passos Gomes, G.; Friederich, P.; Peters, E.; Gaudin, T.; Pollice, R.; Jorner, K.; Nigam, A.; D'Addario, M. L.; Sigman, M. S.; Aspuru-Guzik, A. A Comprehensive Discovery Platform for Organophosphorus Ligands for Catalysis. *J. Am. Chem. Soc.* **2022**, *144*, 1205-1217.

5. Clavier, H.; Nolan, S. P. Percent buried volume for phosphine and *N*-heterocyclic carbene ligands: steric properties in organometallic chemistry. *Chem. Commun.* **2010**, *46*, 841-861.

6. Dai, X.; Chen, Y.; Garrell, S.; Liu, H.; Zhang, L.-K.; Palani, A.; Hughes, G.; Nargund, R. Ligand-Dependent Site-Selective Suzuki Cross-Coupling of 3,5-Dichloropyridazines. *J. Org. Chem.* **2013**, *78*, 7758-7763.

7. Gao, Q.; Yan, H.; Wu, M.; Sun, J.; Yan, X.; Wu, A. Direct synthesis of 2-methylpyridines via I_2-triggered [3 + 2 + 1] annulation of aryl methyl ketoxime acetates with triethylamine as the carbon source. *Org. Biomol. Chem.* **2018**, 16, 2342-2348

8. Petersen, T. P.; Becker, M. R.; Knochel, P. Continuous flow magnesiation of functionalized heterocycles and acrylates with TMPMgCl·LiCl. *Angew. Chem. Int. Ed.* **2014**, *53*, 7933-7937.

9. (a) Scott, N. W. J.; Ford, M. J.; Jeddi, N.; Eyles, A.; Simon, L.; Whitwood, A. C.; Tanner, T.; Willans, C. E.; Fairlamb, I. J. S. A Dichotomy in Cross-Coupling Site Selectivity in a Dihalogenated Heteroarene: Influence of Mononuclear Pd, Pd Clusters, and Pd Nanoparticles—the Case for Exploiting Pd Catalyst Speciation. *J. Am. Chem. Soc.* **2021**, *143*, 9682-9693. (b) Appleby, K. M.; Dzotsi, E.; Scott, N. W. J.; Dexin, G.; Jeddi, N.; Whitwood, A. C.; Pridmore, N. E.; Hart, S.; Duckett, S. B.; Fairlamb, I. J. S. Bridging the Gap from Mononuclear Pd^{II} Precatalysts to Pd Nanoparticles: Identification of Intermediate Linear $[Pd_3(XPh_3)_4]^{2+}$ Clusters as Catalytic Species for Suzuki–Miyaura Couplings (X = P, As). *Organometallics* **2021**, *40*, 3560-3570.

10. Gaussian 16, Revision C.01, Frisch, M. J.; Trucks, G. W.; Schlegel, H. B.; Scuseria, G. E.; Robb, M. A.; Cheeseman, J. R.; Scalmani, G.; Barone, V.; Petersson, G. A.; Nakatsuji, H.; Li, X.; Caricato, M.; Marenich, A. V.; Bloino, J.; Janesko, B. G.; Gomperts, R.; Mennucci, B.; Hratchian, H. P.; Ortiz, J. V.; Izmaylov, A. F.; Sonnenberg, J. L.; Williams-Young, D.; Ding, F.; Lipparini, F.; Egidi, F.; Goings, J.; Peng, B.; Petrone, A.; Henderson, T.; Ranasinghe, D.; Zakrzewski, V. G.; Gao, J.; Rega, N.; Zheng, G.; Liang, W.; Hada, M.; Ehara, M.; Toyota, K.; Fukuda, R.; Hasegawa, J.; Ishida, M.; Nakajima, T.; Honda, Y.; Kitao, O.; Nakai, H.; Vreven, T.; Throssell, K.; Montgomery, J. A., Jr.; Peralta, J. E.; Ogliaro, F.; Bearpark, M. J.; Heyd, J. J.; Brothers, E. N.; Kudin, K. N.; Staroverov, V. N.; Keith, T. A.; Kobayashi, R.; Normand, J.; Raghavachari, K.; Rendell, A. P.; Burant, J. C.; Iyengar, S. S.; Tomasi, J.; Cossi, M.; Millam, J. M.; Klene, M.; Adamo, C.; Cammi, R.; Ochterski, J. W.; Martin, R. L.; Morokuma, K.; Farkas, O.; Foresman, J. B.; Fox, D. J. Gaussian, Inc., Wallingford CT, 2016

11. Cossi, M.; Rega, N.; Scalmani, G.; Barone, V. Energies, structures, and electronic properties of molecules in solution with the C-PCM solvation model. *J. Comput. Chem.* **2003**, *24*, 669-681.

12. Yu, H. S.; He, X.; Truhlar, D. G. MN15-L: A New Local Exchange-Correlation Functional for Kohn–Sham Density Functional Theory with Broad Accuracy for Atoms, Molecules, and Solids. *J. Chem. Theory Comput.* **2016**, *12*, 1280-1293.

13. Hay, P. J.; Wadt, W. R. Ab initio effective core potentials for molecular calculations. Potentials for K to Au including the outermost core orbitals. *J. Chem. Phys.* **1985**, *82*, 299-310.

14. (a) Gonzalez, C.; Schlegel, H. B. An improved algorithm for reaction path following. *J. Chem. Phys.* **1989**, *90*, 2154-2161; (b) Gonzalez, C.; Schlegel, H.B. Reaction Path Following In Mass-Weighted Internal Coordinates. *J. Phys. Chem.* **1990**, *94*, 5523-5527; (c) Fukui, K. The path of chemical reactions - the IRC approach. *Acc. Chem. Res.* **1981**, *14*, 363-368.

15. Yu, H. S.; He, X.; Li, S. L.; Truhlar, D. G. MN15: A Kohn–Sham global-hybrid exchange–correlation density functional with broad accuracy for multi-reference and single-reference systems and noncovalent interactions. *Chem. Sci.* **2016**, *7*, 5032-5051.

16. (a) Dolg, M.; Wedig, U.; Stoll, H.; Preuss, H. Energy-adjusted ab initio pseudopotentials for the first row transition elements. *J. Chem. Phys.* **1987**, *86*, 866-872; (b) Andrae, D.; Haussermann, U.; Dolg, M.; Stoll, H. Preuss, H. Energy-adjusted ab initio pseudopotentials for the second and third row transition elements. *Theor. Chim. Acta* **1990**, *77*, 123-141.

17. Ribeiro, R. F.; Marenich, A. V.; Cramer, C. J.; Truhlar, D. G. Use of Solution-Phase Vibrational Frequencies in Continuum Models for the Free Energy of Solvation. *J. Phys. Chem. B.* **2011**, *115*, 14556-14562.

18. G. Luchini, J. V. Alegre- Requena, I. Funes-Ardoiz and R. S. Paton, GoodVibes: Automated Thermochemistry for Heterogeneous Computational Chemistry Data, *F1000Research*, **2020**, *9*, 291

19. CYLview20; Legault, C. Y., Université de Sherbrooke, 2020 (http://www.cylview.org)

20. (a) Avogadro: an open-source molecular builder and visualization tool. Version 1. http://avogadro.cc/ (b) Hanwell, M. D.; Curtis, D. E.; Lonie, D. C.; Vandermeersch, T.; Zurek, E.; Hutchison; G. R. Avogadro: An advanced semantic chemical editor, visualization, and analysis platform. *J. Cheminformatics* **2012**, *4*, 17.

21. Melvin, P. R.; Nova, A.; Balcells, D.; Dai, W.; Hazari, N.; Hruszkewycz, D. P.; Shah, H. P.; Tudge, M. T. Design of a Versatile and Improved Precatalyst Scaffold for Palladium-Catalyzed Cross-Coupling: $(\eta^3\text{-}1\text{-}^t\text{Bu-indenyl})_2(\mu\text{-Cl})_2\text{Pd}_2$. *ACS Catal.* **2015**, *5*, 3680-3688.

22. Moltved, K. A.; Kepp, K. P. Chemical Bond Energies of 3d Transition Metals Studied by Density Functional Theory. *J. Chem. Theory Comput.* **2018**, *14*, 3479-3492.

23. Elias, E. K.; Rehbein, S. M.; Neufeldt, S. R. Solvent coordination to palladium can invert the selectivity of oxidative addition. *Chem. Sci.* **2022**, *13*, 1618-1628.

24. Joshi, C.; Macharia, J. M.; Izzo, J. A.; Wambua, V.; Kim, S.; Hirschi, J. S.; Vetticatt, M. J. Isotope Effects Reveal the Catalytic Mechanism of the Archetypical Suzuki-Miyaura Reaction. *ACS Catal.* **2022**, *12*, 2959-2966.

25. Besora, M.; Maseras, F. The diverse mechanisms for the oxidative addition of C–Br bonds to $Pd(PR_3)$ and $Pd(PR_3)_2$ complexes. *Dalton Trans.* **2019**, *48*, 16242-16248.

26. Lu, J.; Donnecke, S.; Paci, I.; Leitch, D. C. A reactivity model for oxidative addition to palladium enables quantitative predictions for catalytic cross-coupling reactions. *Chem. Sci.* **2022**, *13*, 3477-3488.

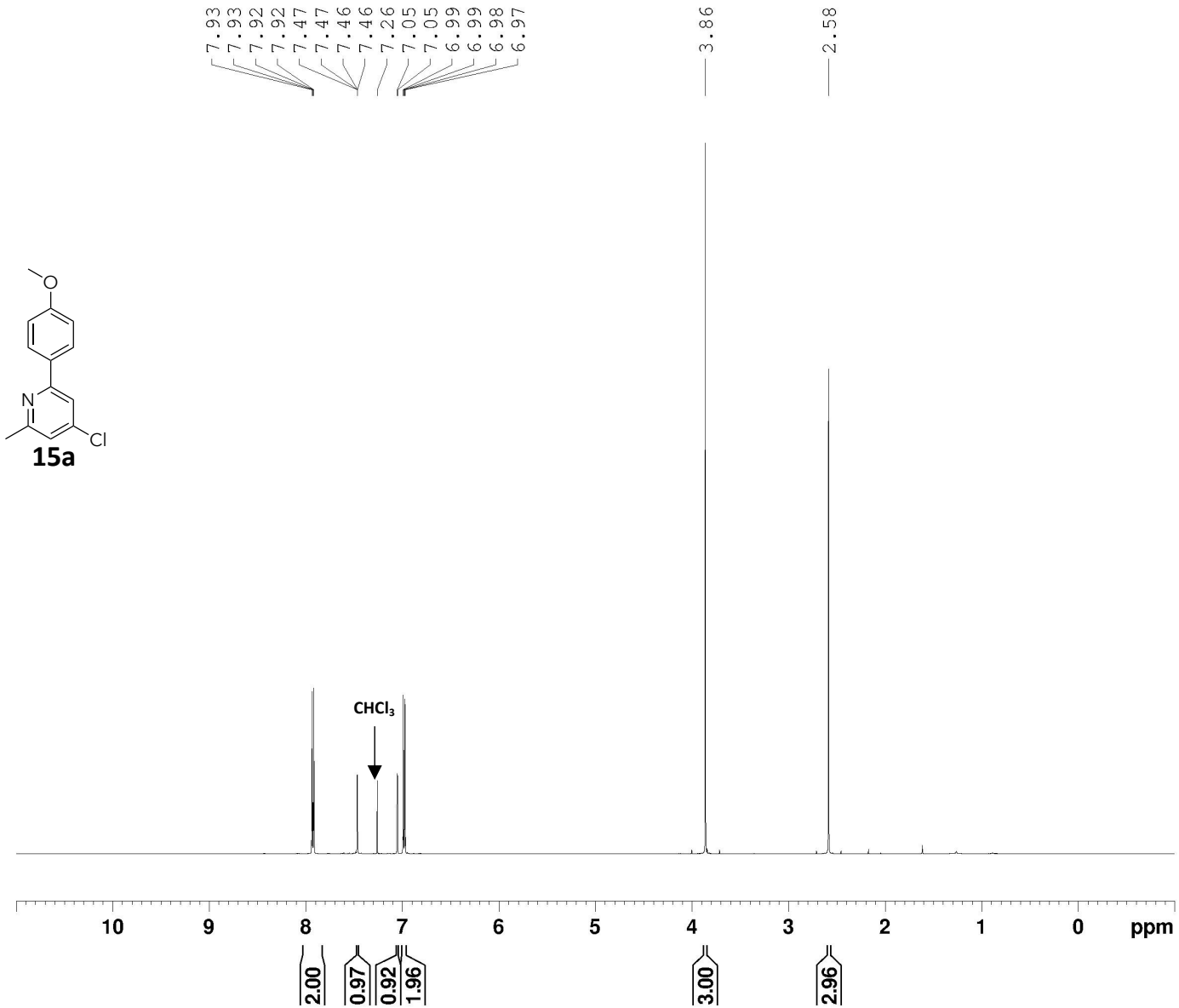


```
Current Data Parameters
NAME      NL-1-171-f11-13
EXPNO                  10
PROCNO                  1

F2 - Acquisition Parameters
Date_           20220214
Time               10.17 h
INSTRUM            spect
PROBHD   Z125869_0055 (
PULPROG             zg30
TD                 65536
SOLVENT            CDCl3
NS                    64
DS                     2
SWH            10000.000 Hz
FIDRES          0.305176 Hz
AQ             3.2767999 sec
RG                 94.51
DW                50.000 usec
DE                 16.00 usec
TE                 298.0 K
D1            2.00000000 sec
TD0                    1
SFO1         500.2330889 MHz
NUC1                  1H
P0                  4.00 usec
P1                 12.00 usec
PLW1         11.44699955 W

F2 - Processing parameters
SI                 65536
SF          500.2300120 MHz
WDW                   EM
SSB                    0
LB                  0.30 Hz
GB                     0
PC                  1.00
```

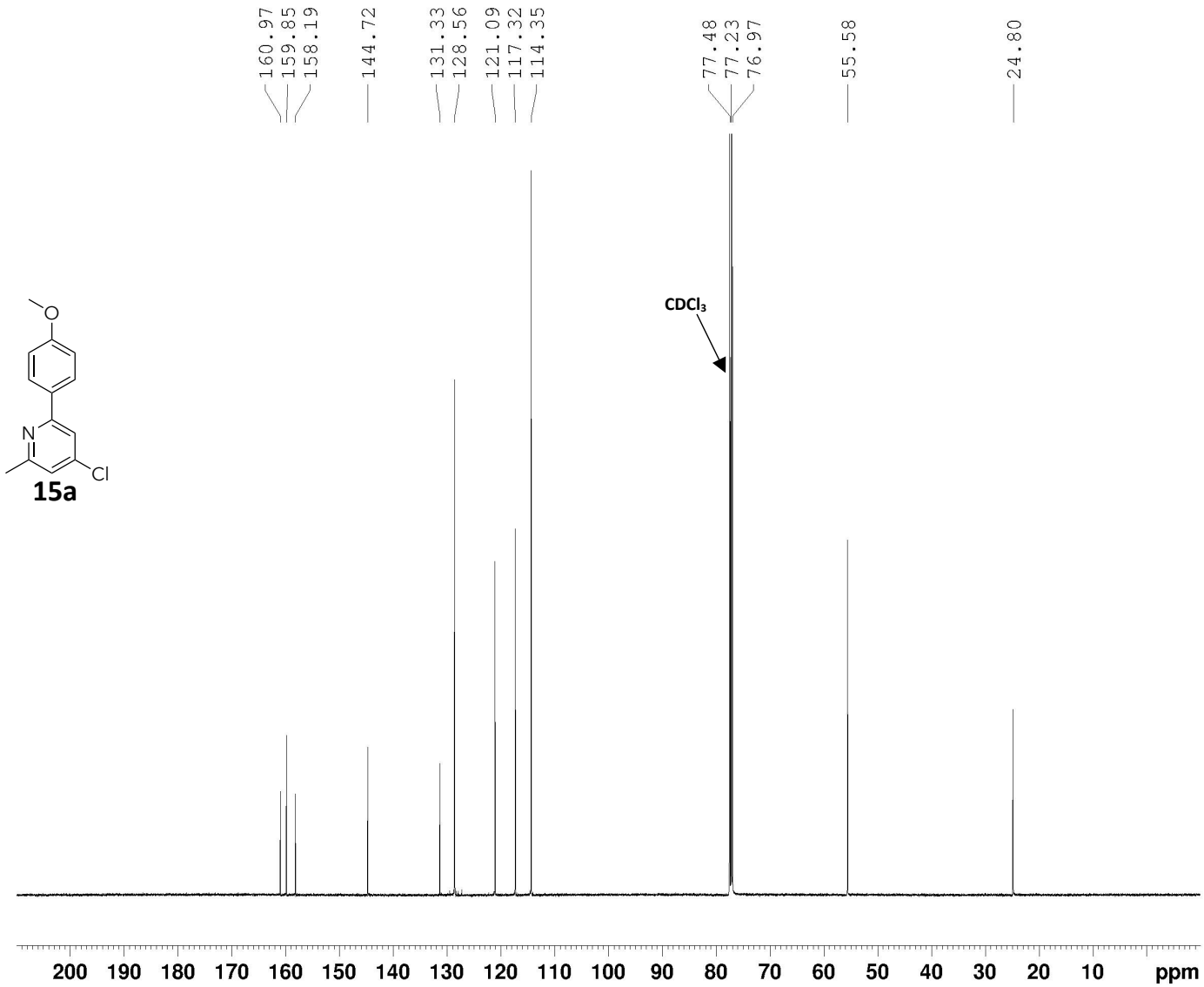


```
Current Data Parameters
NAME      NL-1-171-f11-13
EXPNO                  11
PROCNO                  1

F2 - Acquisition Parameters
Date_           20220214
Time              18.57 h
INSTRUM           spect
PROBHD   Z125869_0055 (
PULPROG          zgpg30
TD                65536
SOLVENT           CDCl3
NS                 1024
DS                    4
SWH           29761.904 Hz
FIDRES         0.908261 Hz
AQ            1.1010048 sec
RG               190.44
DW               16.800 usec
DE               18.00 usec
TE               298.0 K
D1           2.00000000 sec
D11          0.03000000 sec
TD0                    1
SFO1        125.7955118 MHz
NUC1                13C
P0                 3.33 usec
P1               10.00 usec
PLW1        56.90299988 W
SFO2        500.2320009 MHz
NUC2                 1H
CPDPRG[2        waltz16
PCPD2            80.00 usec
PLW2        11.44699955 W
PLW12        0.25756001 W
PLW13        0.12955000 W

F2 - Processing parameters
SI                32768
SF        125.7829086 MHz
WDW                  EM
SSB                   0
LB                 1.00 Hz
GB                    0
PC                 1.40
```

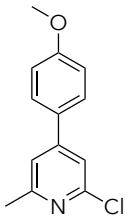

15b

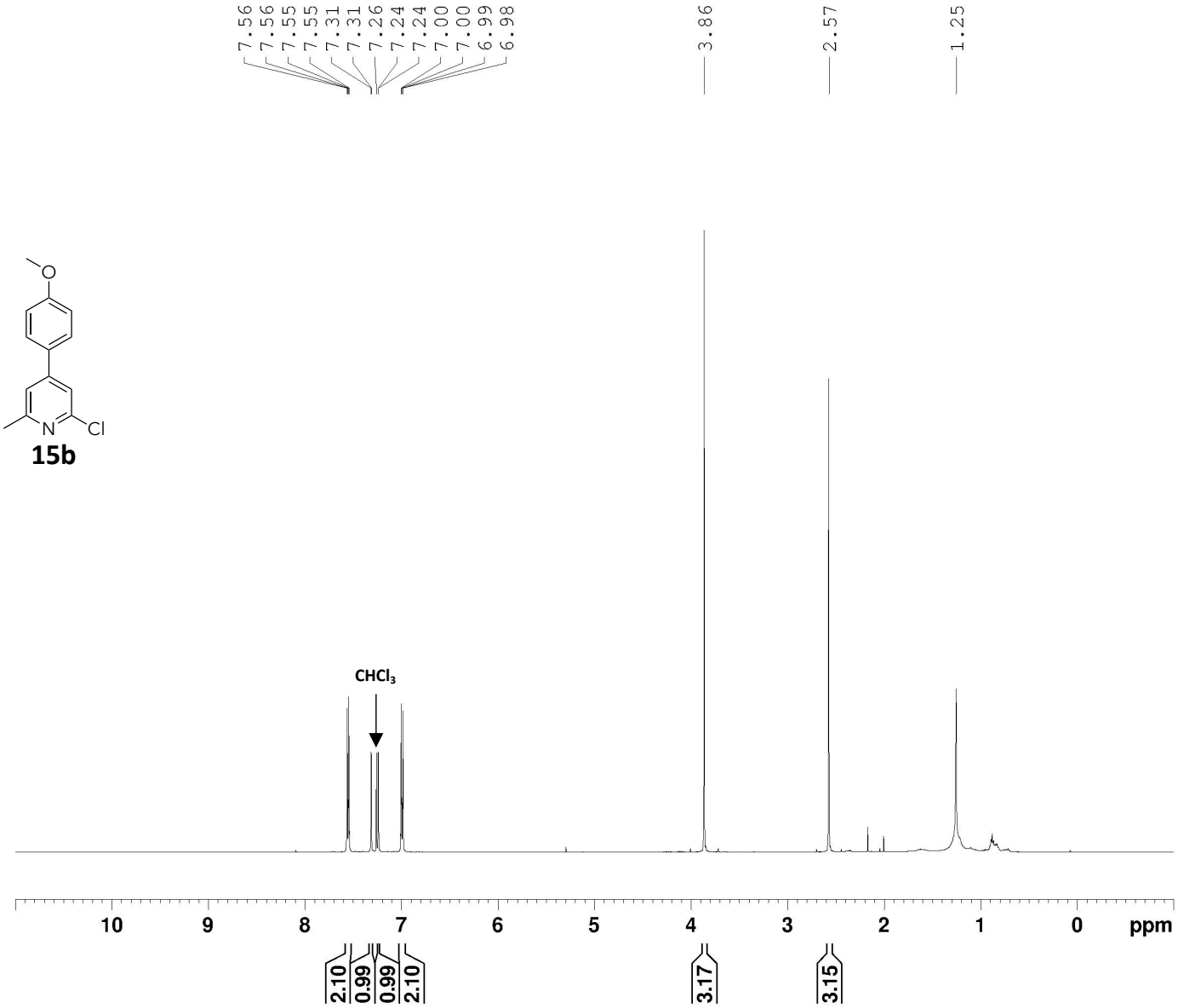


```
Current Data Parameters
NAME        NL-1-172.1-1H
EXPNO                  10
PROCNO                  1

F2 - Acquisition Parameters
Date_            20220216
Time                12.19 h
INSTRUM             spect
PROBHD    Z125869_0055 (
PULPROG              zg30
TD                  65536
SOLVENT             CDCl3
NS                     64
DS                      2
SWH             10000.000 Hz
FIDRES           0.305176 Hz
AQ              3.2767999 sec
RG                  94.51
DW                 50.000 usec
DE                 16.00 usec
TE                 298.0 K
D1             2.00000000 sec
TD0                     1
SFO1          500.2330889 MHz
NUC1                   1H
P0                  4.00 usec
P1                 12.00 usec
PLW1          11.44699955 W

F2 - Processing parameters
SI                  65536
SF            500.2300121 MHz
WDW                    EM
SSB                     0
LB                   0.30 Hz
GB                      0
PC                   1.00
```

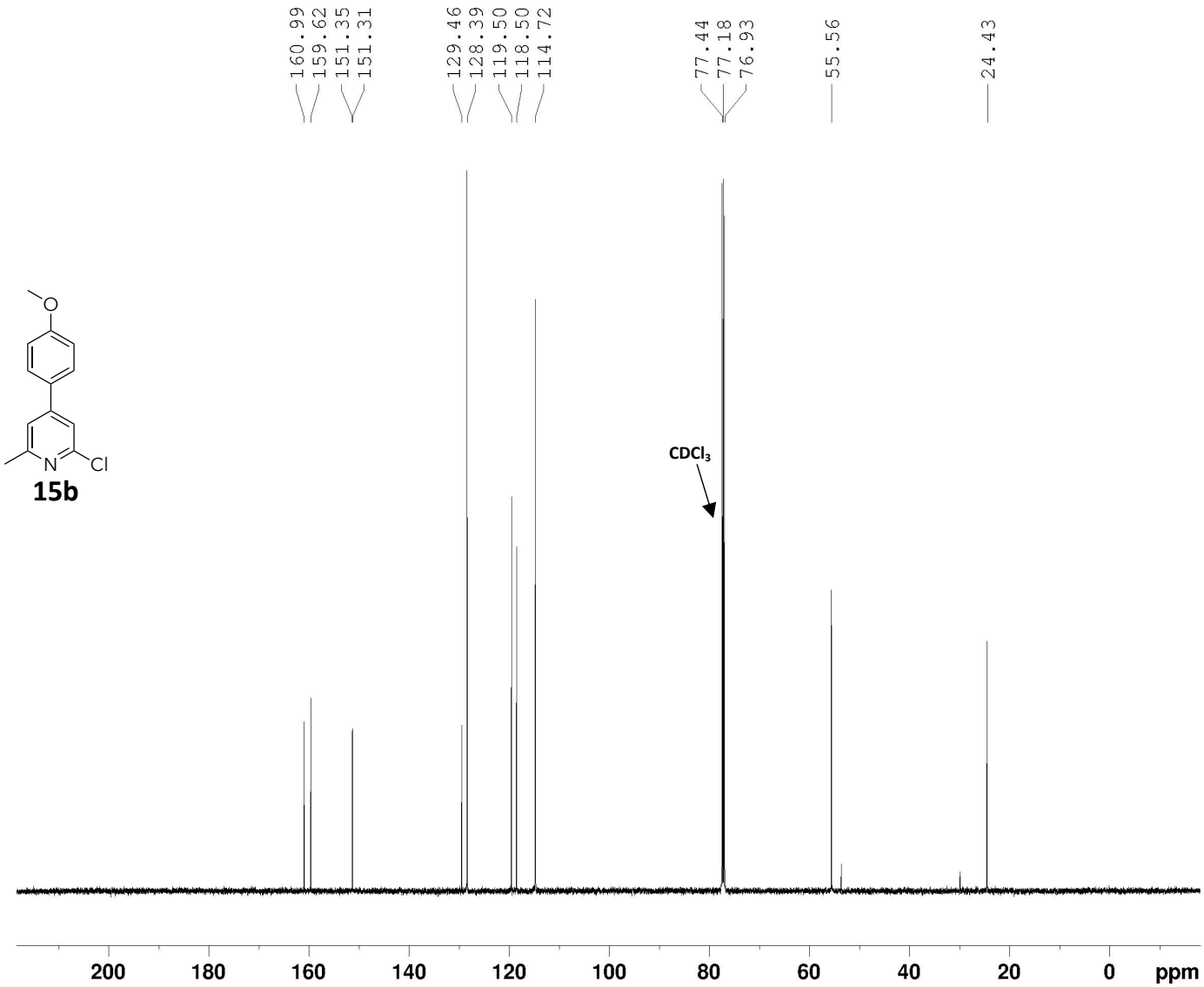


```
Current Data Parameters
NAME        NL-1-172-13C
EXPNO                 10
PROCNO                 1

F2 - Acquisition Parameters
Date_           20220216
Time               11.07 h
INSTRUM            spect
PROBHD   Z125869_0055 (
PULPROG          zgpg30
TD                65536
SOLVENT           CDCl3
NS                   64
DS                    4
SWH            29761.904 Hz
FIDRES          0.908261 Hz
AQ             1.1010048 sec
RG                190.44
DW                16.800 usec
DE                 18.00 usec
TE                 298.0 K
D1            2.00000000 sec
D11           0.03000000 sec
TD0                    1
SFO1         125.7955118 MHz
NUC1                 13C
P0                  3.33 usec
P1                 10.00 usec
PLW1         56.90299988 W
SFO2         500.2320009 MHz
NUC2                  1H
CPDPRG[2         waltz16
PCPD2              80.00 usec
PLW2         11.44699955 W
PLW12         0.25756001 W
PLW13         0.12955000 W

F2 - Processing parameters
SI                 32768
SF         125.7829166 MHz
WDW                   EM
SSB                    0
LB                  1.00 Hz
GB                     0
PC                  1.40
```

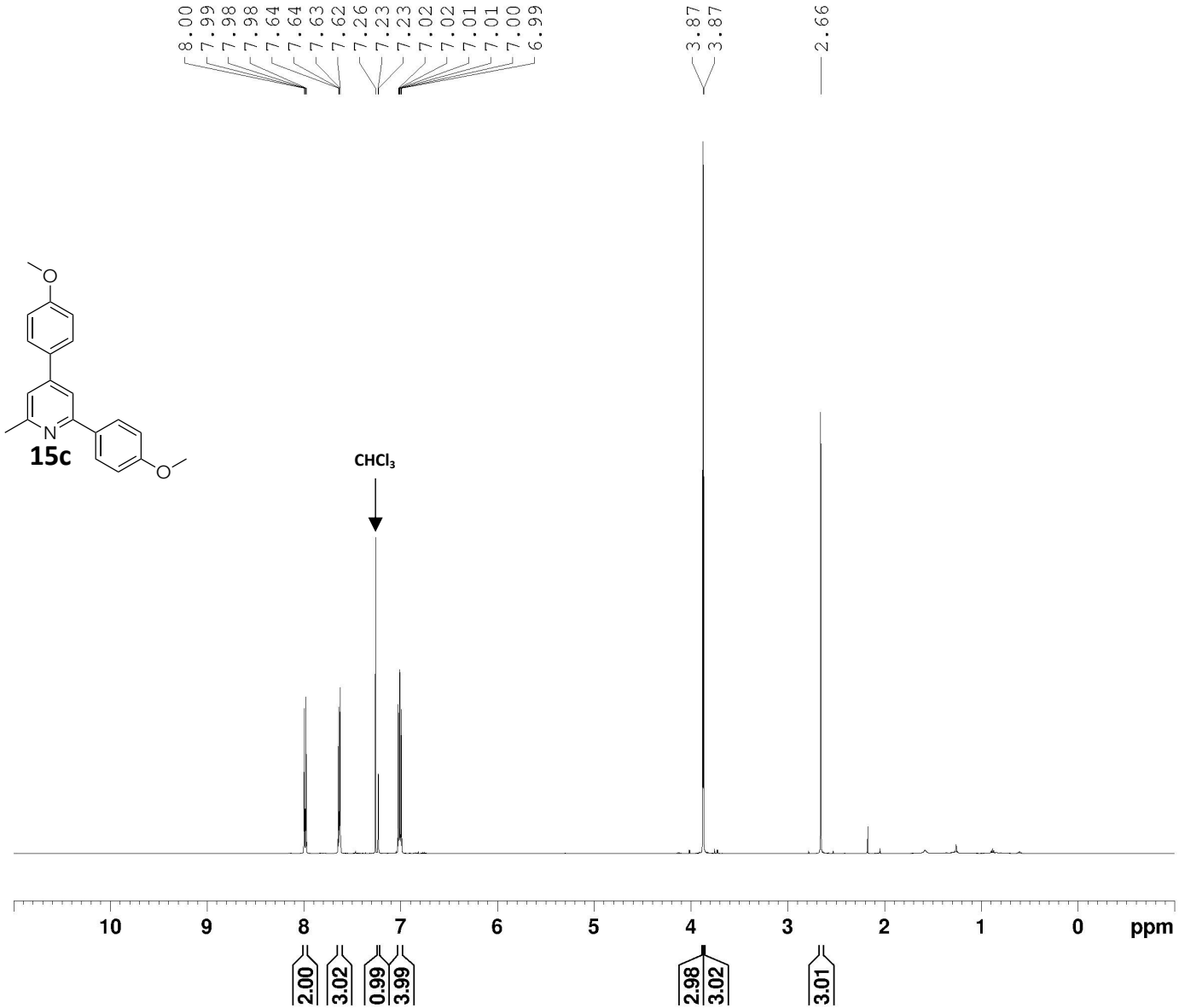


```
Current Data Parameters
NAME          NL-1-133-2
EXPNO                 11
PROCNO                 1

F2 - Acquisition Parameters
Date_           20220215
Time               21.56 h
INSTRUM            spect
PROBHD   Z125869_0055 (
PULPROG             zg30
TD                 65536
SOLVENT            CDCl3
NS                    64
DS                     2
SWH            10000.000 Hz
FIDRES          0.305176 Hz
AQ             3.2767999 sec
RG                151.18
DW                50.000 usec
DE                 16.00 usec
TE                 298.0 K
D1            2.00000000 sec
TD0                    1
SFO1         500.2330889 MHz
NUC1                  1H
P0                  4.00 usec
P1                 12.00 usec
PLW1         11.44699955 W

F2 - Processing parameters
SI                 65536
SF           500.2300121 MHz
WDW                   EM
SSB                    0
LB                  0.30 Hz
GB                     0
PC                  1.00
```

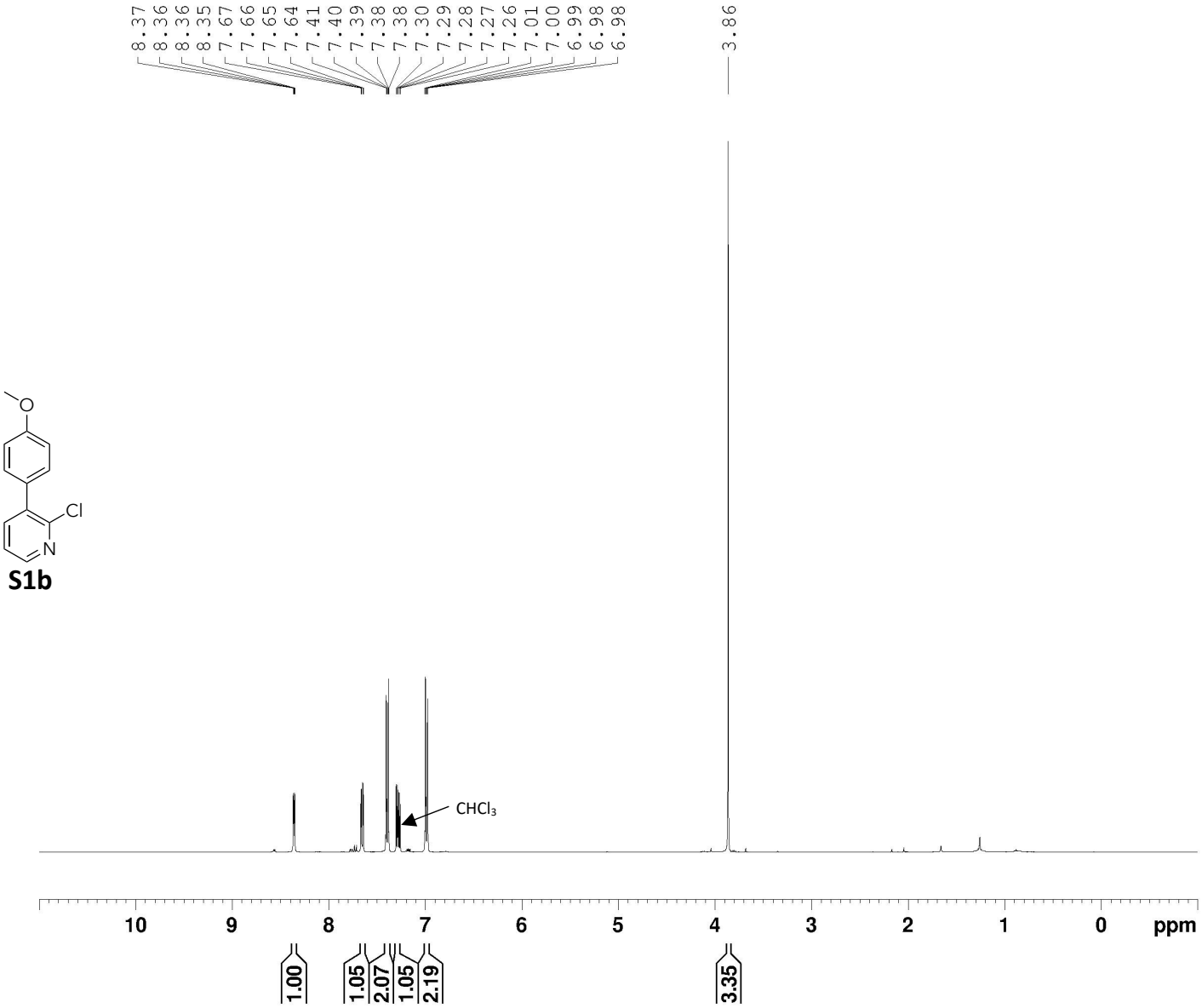


```
Current Data Parameters
NAME        NL-2-2-f12-14
EXPNO                  13
PROCNO                  1

F2 - Acquisition Parameters
Date_            20220331
Time                17.57 h
INSTRUM       Avance Neo
PROBHD    Z152088_0031 (
PULPROG              zg30
TD                  65536
SOLVENT             CDCl3
NS                     16
DS                      2
SWH             8196.722 Hz
FIDRES          0.250144 Hz
AQ             3.9976959 sec
RG                    101
DW                 61.000 usec
DE                 13.89 usec
TE                 298.0 K
D1            1.00000000 sec
TD0                     1
SFO1         400.1324708 MHz
NUC1                   1H
P0                  2.67 usec
P1                  8.00 usec
PLW1         24.03499985 W

F2 - Processing parameters
SI                  65536
SF           400.1300096 MHz
WDW                    EM
SSB                     0
LB                   0.30 Hz
GB                      0
PC                   1.00
```

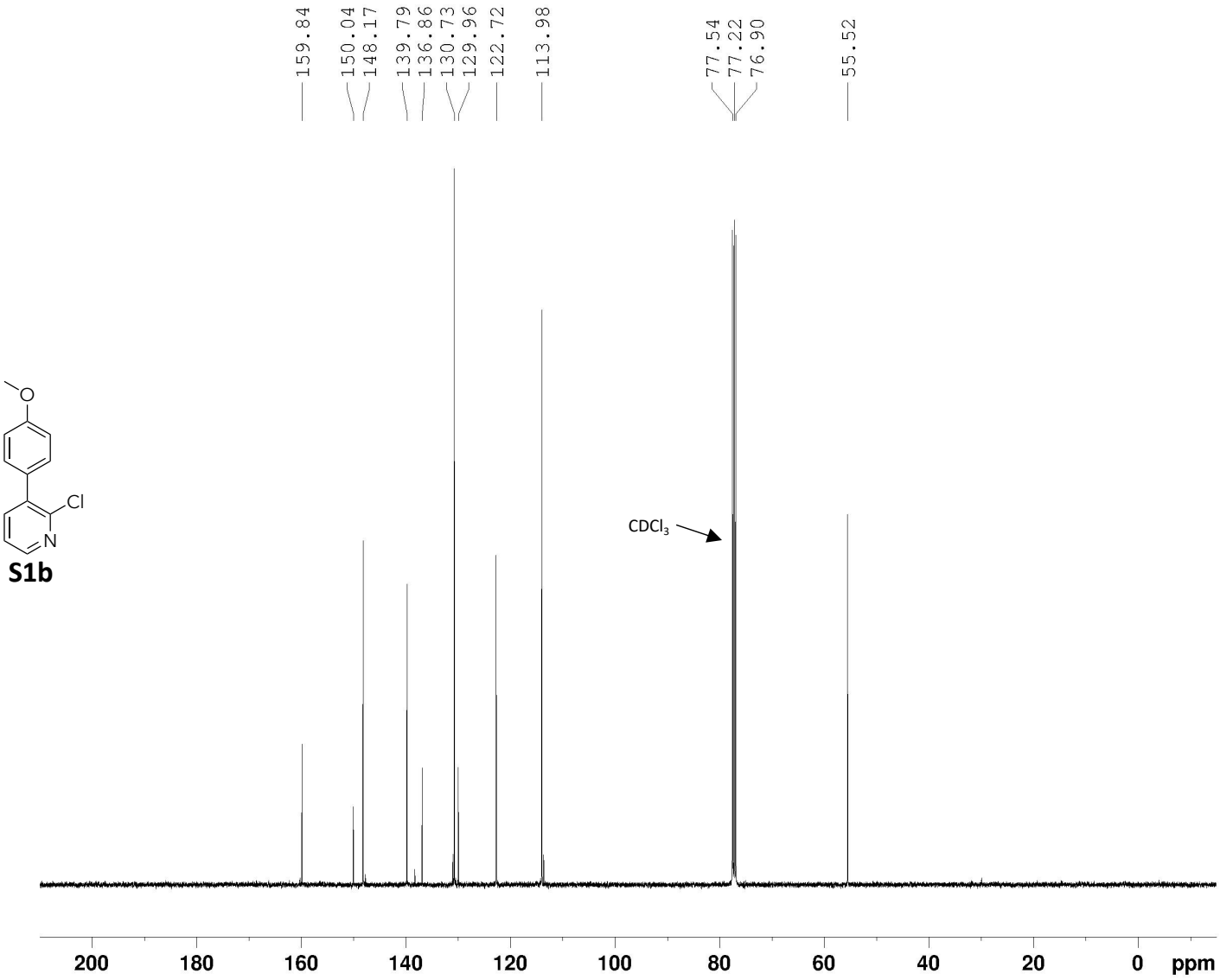


```
Current Data Parameters
NAME       NL-2-2-f12-14
EXPNO                 14
PROCNO                 1

F2 - Acquisition Parameters
Date_           20220331
Time               19.17 h
INSTRUM       Avance Neo
PROBHD   Z152088_0031 (
PULPROG          zgpg30
TD                65536
SOLVENT           CDCl3
NS                 1024
DS                    4
SWH            23809.523 Hz
FIDRES          0.726609 Hz
AQ             1.3762560 sec
RG                 8.125
DW                21.000 usec
DE                 6.50 usec
TE                298.0 K
D1            2.00000000 sec
D11           0.03000000 sec
TD0                    1
SFO1         100.6228298 MHz
NUC1                 13C
P0                 2.67 usec
P1                 8.00 usec
PLW1         86.55400085 W
SFO2         400.1316005 MHz
NUC2                  1H
CPDPRG[2         waltz65
PCPD2             90.00 usec
PLW2         24.03499985 W
PLW12         0.18990999 W
PLW13         0.09552100 W

F2 - Processing parameters
SI                32768
SF          100.6127503 MHz
WDW                  EM
SSB                   0
LB                 1.00 Hz
GB                    0
PC                 1.40
```